Residual interactions and tilted rotation in odd-odd ^{164}Tm

W. Reviol, L. L. Riedinger, X. Z. Wang, and J.-Y. Zhang
Department of Physics and Astronomy, University of Tennessee, Knoxville, Tennessee 37996-1200

H. J. Jensen, G. B. Hagemann, R. A. Bark,* P. O. Tjøm,† S. Leoni,‡ T. Lönnroth,§ H. Schnack-Petersen, T. Shizuma,** and J. Wrzesinski††
Niels Bohr Institute, University of Copenhagen, Tandem Accelerator Laboratory, Roskilde, Denmark

P. B. Semmes
Tennessee Technological University, Cookeville, Tennessee 38505
(Received 17 September 1998)

High-spin spectroscopy on odd-odd ^{164}Tm has produced new illustrations of departures from the predictions of principal-axis cranking. Among the nine strongly coupled rotational bands observed, four are assigned to the parallel and antiparallel couplings of two configurations $\pi h_{11/2}\nu i_{13/2}$ and $\pi g_{9/2}\nu i_{13/2}$. This represents the first time that the high-spin properties of both couplings can be explored. We find that the measured $B(M1)/B(E2)$ values in the $K=1(\uparrow\downarrow)$ coupling of $\pi h_{11/2}\nu i_{13/2}$ are 50% larger than those in the $K=6$ $(\uparrow\uparrow)$ coupling, and represent the largest seen in this nucleus. Tilted-axis cranking calculations successfully explain the $M1/E2$ ratios in these two bands, while the particle-rotor calculations did not reproduce the full low-K enhancement. No inversion in the signatures of the $K=6$ $\pi h_{11/2}\nu i_{13/2}$ band is observed, but there is a small inversion in the $K=1$ coupling up to $I=17\hbar$ and a large inversion in the $\pi h_{9/2}\nu i_{13/2}$ band up to $I=19\hbar$. Remarkably, particle-rotor calculations with a p-n interaction included are able to reproduce these inversions. A stronger p-n interaction is needed to explain an inversion in the $\pi d_{3/2}\nu i_{13/2}$ band. [S0556-2813(99)03303-8]

PACS number(s): 21.10.Re, 21.60.Ev, 23.20.Lv, 27.70.+q

I. INTRODUCTION

There has been great success in understanding the properties of rotational bands in well-deformed rare-earth nuclei in terms of cranking of a deformed rotor about the principal axis of the nucleus, for both normal and superdeformed excitations. Experiments with multidetector arrays are now allowing the measurement of bands of higher spins and larger excitation energies, which in turn provides the opportunity to explore nuclear properties that represent excursions from the predictions of the standard principal-axis cranking (PAC) models [1]. The study of odd-odd deformed nuclei presents special challenges in this regard, both experimentally in view of the usual difficulty in linking observed bands with the known ground or isomeric states and theoretically where one may need to take into account excursions from cranking around the principal axis and/or effects due to residual proton-neutron interactions not included in the normal cranking models.

This paper describes measurements in odd-odd ^{164}Tm of nine sets of strongly coupled rotational bands, three of which had been seen in the earlier work of Drissi *et al.* [2]. This work provides a unique opportunity to explore issues of tilted-axis cranking (TAC) and of p-n residual interactions. A recent study of the isotone ^{163}Er by Brockstedt *et al.* [3] demonstrated the importance of tilted-axis cranking [4] to explain three-quasiparticle bands of high values of the K quantum number, i.e., $K=\frac{19}{2}$. In odd-odd ^{164}Tm we test how central is the concept of tilted-axis cranking to the properties of bands that have two of these three critical quasiparticle orbits excited, and thus explore the success of this model at the two-quasiparticle level. We assign $K=6$ bands in ^{164}Tm to the $\pi h_{11/2}\nu i_{13/2}$, $\pi g_{7/2}\nu i_{13/2}$, and $\pi g_{7/2}\nu h_{9/2}$ configurations, measure $B(M1)/B(E2)$ ratios in each of these bands, and indeed find that the properties are best explained by tilted cranking. In addition, we observe for the first time in an odd-odd nucleus bands built on both the parallel and the antiparallel (and higher-lying) couplings of the involved proton and neutron orbitals, specifically for the $\pi h_{11/2}\nu i_{13/2}$ and $\pi g_{7/2}\nu i_{13/2}$ configurations. Of special interest is the $\pi h_{11/2}\nu i_{13/2}$ configuration. The $K=1\uparrow\downarrow$ band has $B(M1)/B(E2)$ values larger than the $K=6$ coupling, and this fact can be best explained from the predictions of tilted cranking, as described herein.

The second major finding in this work relates to the energy splitting between the two signatures observed for bands in odd-odd ^{164}Tm. Bengtsson *et al.* [5] first discussed the observed inversion of signatures in $\pi h_{11/2}\nu i_{13/2}$ bands in odd-odd nuclei at $N=89$ and attributed this inversion to a

*Present address: Department of Nuclear Physics, Australian National University, Canberra, ACT 0200, Australia.
†Permanent address: Department of Physics, University of Oslo, Oslo, Norway.
‡Present address: Dipartemento di Fisica, Universita di Milano, 20133 Milano, Italy.
§Permanent address: Department of Physics, Abo Akademi, Finland.
**Present address: Department of Physics and Tandem Accelerator Center, University of Tsukuba, Ibaraki 305-8577, Japan.
††Permanent address: Niewodniczanski Institute of Nuclear Physics, PL-31-342 Cracow, Poland.

small but significant asymmetry in the γ direction ($\gamma>0$). The signature inversion in the $\pi h_{11/2}\nu i_{13/2}$ structure decreases as N increases away from this transition region, and becomes nearly zero for the heavier Tm isotopes [6]. As found earlier [2], there is little or no signature inversion in the $K=6$ $\pi h_{11/2}\nu i_{13/2}$ structure of ^{164}Tm, but we find a very significant inversion in the $\pi h_{9/2}\nu i_{13/2}$ band. While tilted cranking seems to have no effect on this, the selective appearance of signature inversion can be explained by invoking a p-n residual interaction along the lines of that discussed earlier by Semmes and Ragnarsson [7]. A similar degree of signature inversion is also present in ^{162}Tm [8] and ^{174}Ta [9], as discussed recently by Bark *et al.* [10]. In this paper we explore more fully the effect of the p-n residual interaction on various bands in ^{164}Tm. Other approaches are possible, as for example Juneja *et al.* [11] suggest that small amounts of signature inversion can be explained without the inclusion of a p-n interaction or $\gamma>0$ by using the framework of the projected shell model calculations of Hara and Sun [12].

Preliminary results from this work have been published in Refs. [13,14]. The recent works on ^{162}Tm [8,15] and on ^{166}Tm [16–18] are also relevant to the discussion herein.

II. EXPERIMENTAL DETAILS AND DATA ANALYSIS

The final nucleus ^{164}Tm was populated in the ^{150}Nd(^{19}F,5n) reaction at a beam energy of 85 MeV. The experiment was performed at the Niels Bohr Institute Tandem Accelerator with the Nordball detector system consisting of up to 20 Compton-suppressed HPGe detectors (situated in four rings) and a 60 element BaF_2 inner ball [19]. Coincident γ-ray events were collected in two separate measurements, namely with a thin, self-supporting and a backed target. In the thin-target run, the beam was focused on a stack of two self-supporting ^{150}Nd foils, each with a thickness of 0.75 mg/cm^2 and an isotopic enrichment of 97.8%. With all 20 HPGe detectors, a total of 1.3×10^9 double and higher-fold Ge events in prompt coincidence with at least one BaF_2 element was recorded. The backed target consisted of a 1.35 mg/cm^2 thick, isotopically enriched ^{150}Nd foil evaporated onto an Au layer of 8.3 mg/cm^2 thickness. In this case, two of the HPGe detectors were replaced by Ge LEPS detectors with Compton-supressors to ensure sensitivity for important low-energy transitions at the bottom parts of γ-ray cascades. A threshold of four was set for the BaF_2 elements firing coincident with at least two HPGe or LEPS detectors, and a total of 0.7×10^9 events was recorded. Energy and efficiency calibrations of the detectors were done with a mixed radioactive source (^{133}Ba, ^{134}Cs, ^{152}Eu) and the relative γ-ray intensities were taken from Ref. [20].

The data were sorted off-line into two- and three-dimensional γ-ray energy histograms. Prompt coincidences between any of the Ge detectors were defined by a narrow, energy-dependent time gate. For the twofold events additional software conditions on both BaF_2 sum energy and fold were required, in order to enhance high spin states in ^{164}Tm. The twofold events from the backed target run were also analyzed for different time conditions which allowed a search for delayed transitions within a $\sim$130 ns time interval. Analysis of the triple coincidences between the HPGe detectors accounting for $\sim$5% of the total events was important to establish the weaker branches of the γ decay in detail. For the construction of the level scheme, the software package RADWARE [21] was used, which includes the two- and three-dimensional analysis programs ESCL8R and LEVIT8R.

An analysis of directional correlations of γ rays from oriented states (DCO ratios) was performed with the aim of determining multipolarities and multipole mixing ratios for the transitions of interest. The four rings of the Nordball array position detectors at $\Theta_1=37°$ and $\Theta_2=79°$ relative to the beam axis and at the equivalent angles of 143° and 101°, respectively. Thus, the intensities of coincidences between detectors at 79°/101° and 37°/143° have been analyzed. The corresponding experimental DCO ratio is

$$R_{\mathrm{DCO}}=\frac{I_{\gamma_2}^{\Theta_1}(\mathrm{gate}_{\gamma_1}^{\Theta_2})}{I_{\gamma_2}^{\Theta_2}(\mathrm{gate}_{\gamma_1}^{\Theta_1})}. \tag{2.1}$$

As the gating transition, γ_1, lines known to be of stretched quadrupole type were chosen consistently. It is then expected that $R_{\mathrm{DCO}}\sim0.6$ if the coincident transition, γ_2, is a pure stretched dipole transition and $R_{\mathrm{DCO}}\sim1.0$ if γ_1 and γ_2 are of the same multipolarity. As quadrupole transitions, only γ rays of $E2$ character are considered, and mixed transitions are assumed to be of $M1/E2$ type.

III. LEVEL SCHEME

The level scheme of ^{164}Tm obtained in the present work is shown in Figs. 1 and 2. Nine rotational band structures were observed with two signatures each and interlinking transitions among them. The ordering of the γ rays is based on their coincidence relationships and relative intensities. The proposed spin and parity assignments to levels are partially determined by the DCO ratios and the previously known low-spin levels reported by Drissi *et al.* [2]. However, since it was mostly not possible to establish the decay of the band heads of the observed rotational cascades to the ground state, these assignments depend also on systematic comparisons with neighboring nuclei. For the bands 1, 6, and 5, which have been observed prior to this work, the parity assignments of Ref. [2] have been adopted. Most of the nine bands can be related to either the low-lying ($E<40$ keV [2]) $K^\pi=6^-$ $t_{1/2}=5.1$ m isomeric state or the $K^\pi=1^+$ ground state; therefore the level scheme is divided into two parts. Since the present data do not allow a connection between these two parts of the level scheme, we discuss them separately beginning with the yrast band, which is proposed to feed the isomer. For ease of discussion, the bands are labeled 1–9. A list of the γ-ray transitions assigned to ^{164}Tm is given in Table I.I. In Fig. 3, representative coincidence spectra for the three bands previously reported [2] are shown.

A. High-K bands

Compared with the level scheme of Drissi *et al.* [2], the yrast band (labeled 6) has been extended by eight spin units up to $28\hbar$. At the bottom of this band, the strong $\Delta I=1$ transitions compete favorably with the $E2$ crossover transitions, as can be also seen in Fig. 3 (top). Both types of γ rays can be observed down to relatively low transition energies

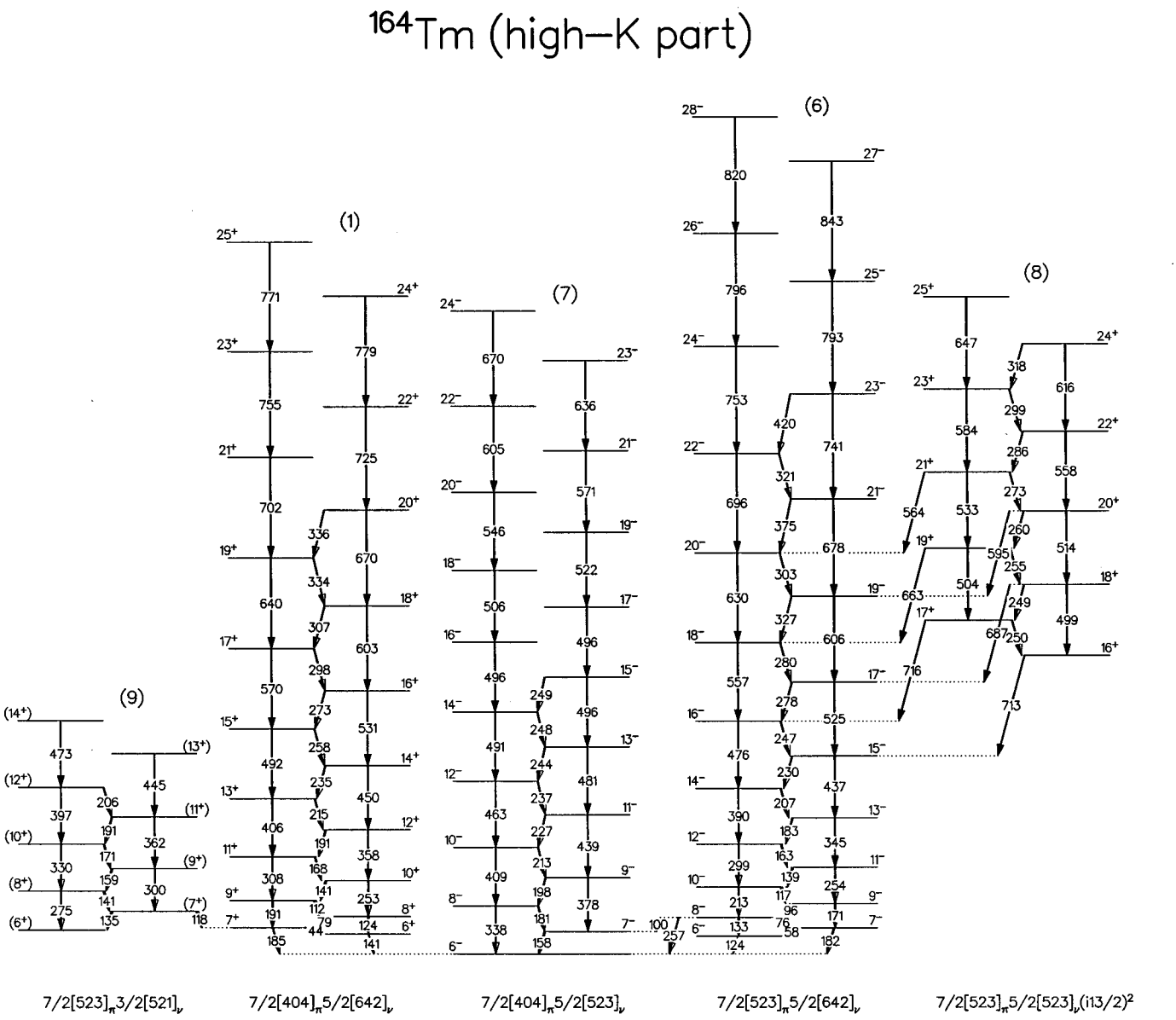

FIG. 1. Proposed level scheme for the high-K bands in ^{164}Tm associated with the 6^- isomeric state ($E<40$ keV [2]). Energies are given in keV. Relative intensities are listed in Table I(a). The assignments of Nilsson quantum numbers to the band heads are discussed in the text.

of, e.g., 58, 75.5 keV ($M1$) and 133.1 keV ($E2$), respectively. This last γ ray has been newly observed and placed in the level scheme on the basis of triple coincidence relationships. To document the low-energy transitions in the cascades forming band 6, we show LEPS spectra gated by a prompt 95.9 keV γ-ray line in Fig. 4(a). The top part of this figure shows the γ-ray transitions in prompt coincidence, while the bottom spectrum is obtained when projecting on γ rays recorded within a time interval of about 10–130 ns (prompt coincidences excluded). By comparison of both spectra, the prompt character of the 75.5 and 58 keV (embedded in the $K_{\beta 2}$ x ray) in-band transitions can be seen. From this example, we may also conclude that the sensitivity for weak or/and significantly converted γ rays allows us to observe the whole band and thus boosts the confidence for the reported spins and excitation energies of the yrast levels. Decay out of the yrast band is observed at $I \leqslant 8$ and proceeds mainly through a 124.2 keV transition delayed by a 36 ns half-life of the $I^\pi = 6^-$ band head state [2]. Its isomeric character is confirmed by the spectrum shown in the bottom part of Fig. 4(a). More decay-out transitions are added to this scheme, with energies of 99.7, 182.2, and 257.3 keV. The latter two transitions bypass the 124 keV γ-ray line, where the measured dipole character of the 182.2 keV transition [cf. Table I(a)] solidifies the proposed spin assignment.

The newly observed band, labeled 7, is linked to band 6 by the aforementioned 99.7 keV transition. The lowest-energy level of this structure is the same 6^- state to which the band 6 decays, namely, the isomer. A representative double-gated spectrum for this relatively weak band is shown in Fig. 5(a). The lowest-lying transitions in band 7 are observed to be of significantly higher energies, as compared to band 6. Thus, with increasing spin band 7 immediately departs from the yrast line. There are also no decay-out transitions from band 7 to lower-lying states observed within the time range of the present coincidence data ($\sim$130 ns). It is therefore reasonable to propose that band 7 is directly based on the 6^- isomer.

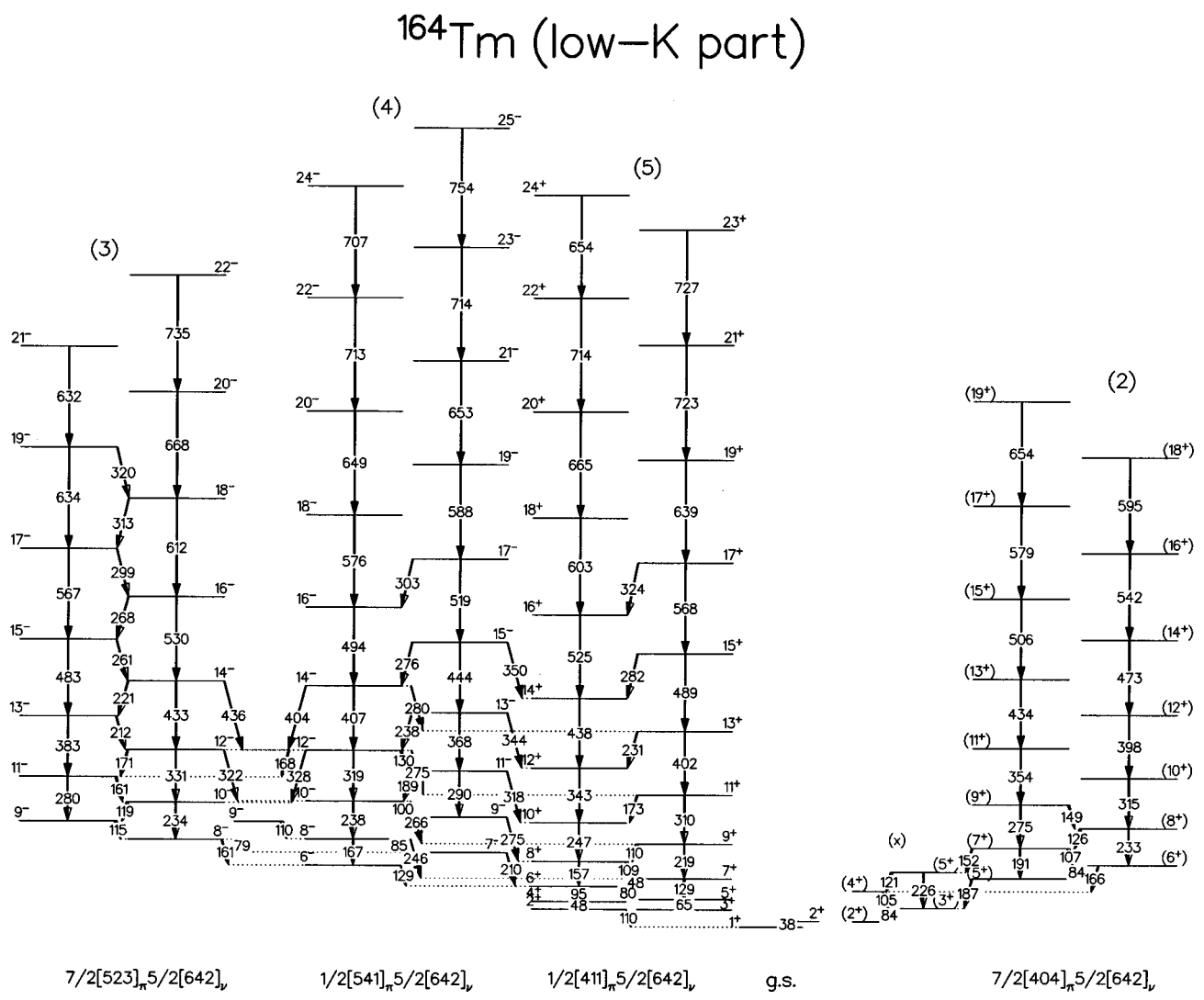

FIG. 2. Proposed level scheme for the low-K bands (associated with the 1^+ ground state) in ^{164}Tm. Energies are given in keV. Relative intensities are listed in Table I(b). The assignments of Nilsson quantum numbers to the band heads are discussed in the text.

Another newly observed band, labeled 8, decays to the yrast band. Figure 5(b) shows a representative spectrum for band 8. This weakly populated structure ends at about 2.1 MeV excitation energy and spin 16. For the linking γ rays with energies of 595.0, 662.7, 687.4, 713.2, and 716.4 keV, DCO ratios consistent with stretched, pure dipoles are measured. This is in accordance with the proposed $E1$ assignments for these interband transitions.

One of the strongest bands is labeled 1, and has been established by Drissi *et al.* [2]. In the present work, this band has been extended to both higher and lower spins. At high spins, it is now known up to $25\hbar$. At low spins, we have added two more in-band transitions with energies of 44 ($M1$) and 123.5 keV ($E2$). These two transitions continue in the rotational-like behavior of the transition energies as a function of spin and most likely feed the band head, which decays via a 141 keV transition to the 6^- isomer. Furthermore, a 185.2 keV $\Delta I=1$ transition is newly observed and can be placed below the 191.0 keV transition at the bottom of the band. This new 185.2 keV transition bypasses the lower-lying 141 keV transition and determines that transition being of I to I type. Similar to the strongest decay-out transition of band 6, this 141 keV transition is somewhat delayed ($t_{1/2}\sim 5$ ns [2]). By analogy, we propose that the head of band 1 has a spin of 6 and most likely decays to the isomer. The proposed positive parity for band 1 rests on model arguments, which are presented in Sec. IV.

Another new structure, labeled 9, has been observed. This band seems to feed into band 1. However, only a weak 117.6 keV linking transition is evident, while the main decay paths of this band remain unobserved. Therefore, we are less confident with spin and parity assignments than for the other bands, as indicated by parentheses.

B. Low-K bands

Rotational bands 4 and 5 are among the most strongly populated level structures in the experiment. Band 5 has been observed previously [2], however not as a signature partner band. The newly observed linking transitions between the $E2$ signature partner sequences have γ-ray energies of 48, 80.2, 109.0, 110.4, 173.1, 230.6, 281.7, and 323.7 keV. The presence of these γ-ray transitions can be seen in the coincidence spectra shown in Figs. 3 (bottom) and 4(b).

TABLE I. (a) Gamma-ray transitions assigned to the high-K part of the level scheme of ^{164}Tm. (b) Gamma-ray transitions assigned to the low-K part of the level scheme of ^{164}Tm.

(a)

E_γ (keV)[a]	I_γ (%)[b]	R_{DCO}	I_i^π	I_f^π	Placement
44			7^+	6^+	band 1
79.2	65	0.82(9)	8^+	7^+	band 1
112.3	96	0.90(1)	9^+	8^+	band 1
123.5	5		8^+	6^+	band 1
141.0	53		10^+	9^+	band 1
140.5			6^+	6^-	band 1, 7
167.5	68	0.91(3)	11^+	10^+	band 1
185.2		0.70(7)	7^+	6^-	band 1, 7
190.6	56	0.96(4)	12^+	11^+	band 1
191.0	44	0.78(4)	9^+	7^+	band 1
214.9	38	0.87(4)	13^+	12^+	band 1
234.7	36	0.86(5)	14^+	13^+	band 1
253.1	99	0.78(4)	10^+	8^+	band 1
257.7	27	0.96(8)	15^+	14^+	band 1
272.6	21	0.97(12)	16^+	15^+	band 1
297.7	15		17^+	16^+	band 1
307.4	10		18^+	17^+	band 1
308.3	136	1.05(4)	11^+	9^+	band 1
333.7	6		19^+	18^+	band 1
336.4	6		20^+	19^+	band 1
358.3	163	1.05(4)	12^+	10^+	band 1
406.2	161	1.09(7)	13^+	11^+	band 1
450.1	144	1.10(7)	14^+	12^+	band 1
492.4	150	1.05(8)	15^+	13^+	band 1
530.7	118	1.06(9)	16^+	14^+	band 1
569.9	111	1.08(9)	17^+	15^+	band 1
603.2	110	1.07(10)	18^+	16^+	band 1
639.9	59	0.99(10)	19^+	17^+	band 1
670.0	46	1.04(10)	20^+	18^+	band 1
701.9	32	1.14(13)	21^+	19^+	band 1
725.0	24		22^+	20^+	band 1
754.7	15		23^+	21^+	band 1
771.1	5		25^+	23^+	band 1
778.6	8		24^+	22^+	band 1
58			7^-	6^-	band 6
75.5	30	0.69(15)	8^-	7^-	band 6
95.9	131	0.78(4)	9^-	8^-	band 6
99.7	17		8^-	7^-	band 6, 7
116.8	279	0.78(4)	10^-	9^-	band 6
124.2			6^-	6^-	band 6, 7
133.1	19		8^-	6^-	band 6
138.5	338	0.83(4)	11^-	10^-	band 6
162.7	312	0.80(4)	12^-	11^-	band 6
170.7	21	0.97(12)	9^-	7^-	band 6
182.2		0.60(15)	7^-	6^-	band 6, 7
183.1	230	0.75(4)	13^-	12^-	band 6
207.4	219	0.82(5)	14^-	13^-	band 6
212.9	64	0.94(10)	10^-	8^-	band 6
229.8	173	0.80(5)	15^-	14^-	band 6
247.1	170	0.81(6)	16^-	15^-	band 6
254.1	121	0.99(7)	11^-	9^-	band 6
257.3	16		8^-	6^-	band 6, 7
278.1	105	0.80(9)	17^-	16^-	band 6

(a)

E_γ (keV)[a]	I_γ (%)[b]	R_{DCO}	I_i^π	I_f^π	Placement
279.5	76	0.80(9)	18^-	17^-	band 6
299.4	113	1.05(7)	12^-	10^-	band 6
303.0	38		20^-	19^-	band 6
320.5	19		22^-	21^-	band 6
326.7	45	0.83(9)	19^-	18^-	band 6
344.8	150	1.05(7)	13^-	11^-	band 6
374.7	22	0.70(10)	21^-	20^-	band 6
389.9	165	1.03(7)	14^-	12^-	band 6
419.7	13		23^-	22^-	band 6
436.6	246	1.09(9)	15^-	13^-	band 6
476.4	203	1.07(8)	16^-	14^-	band 6
524.9	195	1.20(11)	17^-	15^-	band 6
557.1	141	1.08(16)	18^-	16^-	band 6
605.9	129	1.12(18)	19^-	17^-	band 6
630.1	106	1.24(19)	20^-	18^-	band 6
678.3	70		21^-	19^-	band 6
695.6	61	1.26(20)	22^-	20^-	band 6
740.6	29	1.20(21)	23^-	21^-	band 6
753.1	29		24^-	22^-	band 6
792.8	18		25^-	23^-	band 6
795.6	12		26^-	24^-	band 6
820.4	5		28^-	26^-	band 6
843.4	8		27^-	25^-	band 6
158.2			7^-	6^-	band 7
180.6	26		8^-	7^-	band 7
197.6	17		9^-	8^-	band 7
212.6	13		10^-	9^-	band 7
226.8	10		11^-	10^-	band 7
236.6	11		12^-	11^-	band 7
243.8	14		13^-	12^-	band 7
247.6	18		14^-	13^-	band 7
248.8	15		15^-	14^-	band 7
338.3	25		8^-	6^-	band 7
377.8	20		9^-	7^-	band 7
409.3	23		10^-	8^-	band 7
438.7	27		11^-	9^-	band 7
462.8	28		12^-	10^-	band 7
481.3	26		13^-	11^-	band 7
491.3	28		14^-	12^-	band 7
496.3	14		15^-	13^-	band 7
496.4	20		16^-	14^-	band 7
496.4	12		17^-	15^-	band 7
505.9	18		18^-	16^-	band 7
522.3	17		19^-	17^-	band 7
545.5	10		20^-	18^-	band 7
571.0	7		21^-	19^-	band 7
605.0	6		22^-	20^-	band 7
635.5	8		23^-	21^-	band 7
670.0	5		24^-	22^-	band 7
249.1	31		18^+	17^+	band 8
249.7	13		17^+	16^+	band 8
254.8	37		19^+	18^+	band 8
259.9	28		20^+	19^+	band 8

TABLE I. (*Continued*).

(a)						(b)					
E_γ (keV)[a]	I_γ (%)[b]	R_{DCO}	I_i^π	I_f^π	Placement	E_γ (keV)[a]	I_γ (%)[b]	R_{DCO}	I_i^π	I_f^π	Placement
272.8	18		21^+	20^+	band 8	541.5	20		(16^+)	(14^+)	band 2
285.9	31		22^+	21^+	band 8	578.9	16		(17^+)	(15^+)	band 2
298.9			23^+	22^+	band 8	595.4	14		(18^+)	(16^+)	band 2
318.0	14		24^+	23^+	band 8	653.8	3		(19^+)	(17^+)	band 2
499.3	14		18^+	16^+	band 8	79.3			8^-	7^-	band 3, 4
503.8	23		19^+	17^+	band 8	110.0			9^-	8^-	band 3, 4
514.1	28		20^+	18^+	band 8	115.2		0.81(5)	9^-	8^-	band 3
532.5	27		21^+	19^+	band 8	119.3	60	0.80(3)	10^-	9^-	band 3
558.4	33		22^+	20^+	band 8	160.6	109	0.76(3)	11^-	10^-	band 3
584.3	31		23^+	21^+	band 8	161.2			8^-	6^-	band 3, 4
616.4	33		24^+	22^+	band 8	170.7	75	0.78(4)	12^-	11^-	band 3
647.2	24		25^+	23^+	band 8	211.8	81		13^-	12^-	band 3
564.2	12		21^+	20^-	band 8, 6	221.3	42	0.77(4)	14^-	13^-	band 3
595.0	19	0.57(19)	20^+	19^-	band 8, 6	234.2	23		10^-	8^-	band 3
662.7	28	0.68(17)	19^+	18^-	band 8, 6	261.0	53	0.79(4)	15^-	14^-	band 3
687.4	34	0.59(12)	18^+	17^-	band 8, 6	268.1	34	0.83(5)	16^-	15^-	band 3
713.2	39	0.61(21)	16^+	15^-	band 8, 6	280.1	29	1.03(8)	11^-	9^-	band 3
716.4	32	0.60(22)	17^+	16^-	band 8, 6	298.7	36	0.89(10)	17^-	16^-	band 3
117.6	10		(7^+)	(7^+)	band 9, 1	312.6	39	0.78(12)	18^-	17^-	band 3
134.5	5		(7^+)	(6^+)	band 9	319.7	16	0.52(25)	19^-	18^-	band 3
140.9			(8^+)	(7^+)	band 9	321.6	23		12^-	10^-	band 3, 4
159.0	33		(9^+)	(8^+)	band 9	331.2	23	1.14(8)	12^-	10^-	band 3
170.9	26		(10^+)	(9^+)	band 9	383.0	33	1.02(6)	13^-	11^-	band 3
190.5	24		(11^+)	(10^+)	band 9	433.3	39	1.19(8)	14^-	12^-	band 3
206.2	23		(12^+)	(11^+)	band 9	435.6	29		14^-	12^-	band 3, 4
274.8	14		(8^+)	(6^+)	band 9	483.1	41	1.03(8)	15^-	13^-	band 3
299.9	29		(9^+)	(7^+)	band 9	529.6	45	1.07(12)	16^-	14^-	band 3
330.2	17		(10^+)	(8^+)	band 9	567.1	43	1.13(17)	17^-	15^-	band 3
361.6	12		(11^+)	(9^+)	band 9	612.0	43	1.18(18)	18^-	16^-	band 3
396.6	22		(12^+)	(10^+)	band 9	633.6	26	1.12(20)	19^-	17^-	band 3
445.2	19		(13^+)	(11^+)	band 9	667.5	26		20^-	18^-	band 3
472.8	22		(14^+)	(12^+)	band 9	632.2	19		21^-	19^-	band 3
(b)						735.3	9		22^-	20^-	band 3
83.9	2		(6^+)	(5^+)	band 2	84.9			8^-	7^-	band 4
84			(3^+)	(2^+)	band x	99.7	3		10^-	9^-	band 4
104.8	13		(4^+)	(3^+)	band x	128.6			6^-	4^+	band 4, 5
107.1	2		(7^+)	(6^+)	band 2	129.7	18		12^-	11^-	band 4
121.4	6		(5^+)	(4^+)	band x	166.9	2		8^-	6^-	band 4
125.9	3		(8^+)	(7^+)	band 2	167.7	55		12^-	11^-	band 4, 3
148.8	3		(9^+)	(8^+)	band 2	189.1	19		11^-	10^-	band 4
151.7	9		(7^+)	(5^+)	band 2, *x*	209.8			7^-	6^+	band 4, 5
165.8	11		(6^+)	(4^+)	band 2, *x*	237.8	11		10^-	8^-	band 4
186.7	9		(5^+)	(3^+)	band 2, *x*	238.1	28		13^-	12^-	band 4
191.1	10		(7^+)	(5^+)	band 2	245.9	12		8^-	7^+	band 4, 5
226.0	7		(5^+)	(3^+)	band x	265.6	20	0.63(9)	10^-	9^+	band 4, 5
233.3	19		(8^+)	(6^+)	band 2	274.7	11		9^-	8^+	band 4, 5
275.4	19		(9^+)	(7^+)	band 2	274.5	14	0.60(12)	12^-	11^+	band 4, 5
315.1	20		(10^+)	(8^+)	band 2	275.6	33		15^-	14^-	band 4
354.3	22		(11^+)	(9^+)	band 2	279.7	11	0.62(9)	14^-	13^+	band 4, 5
398.2	22		(12^+)	(10^+)	band 2	290.3	15		11^-	9^-	band 4
433.8	23		(13^+)	(11^+)	band 2	302.7	9		17^-	16^-	band 4
473.3	22		(14^+)	(12^+)	band 2	318.2	24		11^-	10^+	band 4, 5
506.4	22		(15^+)	(13^+)	band 2	319.4	48		12^-	10^-	band 4

TABLE I. (*Continued*).

(b)						(b)					
E_γ (keV)[a]	I_γ (%)[b]	R_{DCO}	I_i^π	I_f^π	Placement	E_γ (keV)[a]	I_γ (%)[b]	R_{DCO}	I_i^π	I_f^π	Placement
328.1	27		12^-	10^-	band 4, 3	110.4	15	0.66(10)	9^+	8^+	band 5
343.7	35		13^-	12^+	band 4, 5	128.6	116	0.87(8)	7^+	5^+	band 5
349.7	13	0.60(14)	15^-	14^+	band 4, 5	156.6	150		8^+	6^+	band 5
368.4	33		13^-	11^-	band 4	173.1	19		11^+	10^+	band 5
403.7	24		14^-	12^-	band 4, 3	218.7	150	0.90(4)	9^+	7^+	band 5
407.4	163		14^-	12^-	band 4	230.6	18	0.62(7)	13^+	12^+	band 5
443.8	48		15^-	13^-	band 4	246.6	261	1.12(4)	10^+	8^+	band 5
493.6	145		16^-	14^-	band 4	281.7	10		15^+	14^+	band 5
519.3	43		17^-	15^-	band 4	310.3	162	0.97(5)	11^+	9^+	band 5
575.6	105		18^-	16^-	band 4	323.7	7		17^+	16^+	band 5
588.3	42		19^-	17^-	band 4	343.4	252		12^+	10^+	band 5
652.5	34		21^-	19^-	band 4	401.6	142		13^+	11^+	band 5
648.9	64		20^-	18^-	band 4	437.8	209	1.19(6)	14^+	12^+	band 5
707.4	11		24^-	22^-	band 4	488.5	118		15^+	13^+	band 5
713.3	29		22^-	20^-	band 4	525.4	146		16^+	14^+	band 5
713.6	13		23^-	21^-	band 4	568.0	98		17^+	15^+	band 5
754.3	5		25^-	23^-	band 4	603.0	114		18^+	16^+	band 5
48			4^+	2^+	band 5	638.9	59		19^+	17^+	band 5
48			7^+	6^+	band 5	653.5	5		24^+	22^+	band 5
65		0.94(14)	5^+	3^+	band 5	664.8	62		20^+	18^+	band 5
80.2	1	0.63(13)	6^+	5^+	band 5	713.5	16		22^+	20^+	band 5
95.3	8		6^+	4^+	band 5	723.0	16		21^+	19^+	band 5
109.0	7		8^+	7^+	band 5	727.4	5		23^+	21^+	band 5
110.1			2^+	1^+	band 5,gs						

[a]Typical uncertainties on the γ-ray energies are 0.3 keV for the strongest transitions and up to 0.7 keV for the weakest transitions.
[b]Typical uncertainties on the γ-ray intensities are 3% for the strongest transitions and up to 10% for the weakest transitions.

Notice that the 48 keV γ ray has been found to be a doublet. For most of these linking transitions, DCO ratios could be obtained, which are all supportive of $M1$ assignments. Compared to the previous work [2], band 5 has been significantly extended towards both higher and lower spins. At low spins, one and two more $E2$ transitions have been added to the signature partner sequences. These are the transitions with energies of 48, 65, and 95.3 keV, respectively. Band 5 is tentatively connected to the $I^\pi = 1^+$ ground state by a 110 keV transition. As indicated by the two coincidence gates on the 218.7 keV transition shown in Fig. 4(b), evidence for a 110 keV transition below band 5 is obtained in the delayed time window. Furthermore, this delayed 110 keV transition is seen to be in anticoincidence with both the 65 keV $5^+ \rightarrow 3^+$ transition and a 37.5 keV transition that presumably feeds the 1^+ ground state [2]. Information on the angular distribution of the delayed 110 keV transition is obtained, suggesting dipole character. However, this 110 keV transition is complicated by the presence of another 110 keV γ ray due to Coulomb excitation of ^{19}F (beam). There is possibly a transition of 70 keV from the 3^+ state to the 2^+ state (at 37.5 keV [2]). Unfortunately, this 70 keV line cannot be conclusively placed in the scheme, since it overlaps with the 69 keV Au x ray (target backing). Nevertheless, the most likely scenario for the decay-out appears to be a 110 keV $M1$ transition to the 1^+ ground state, and this determines the spins of band 5 as well as of the bands 4 and 3. The proposed positive parity for band 5 rests on model arguments, which are presented in Sec. IV.

A representative coincidence spectrum for the newly observed band 4 is shown in Fig. 5(d). This band decays to band 5 through a series of transitions with energies of 245.9, 265.6, 274.5, 274.7, 279.7, 318.2, 343.7, and 349.7 keV. The DCO ratios obtained for these transitions are consistently around 0.6, which requires dipole assignments. The apparent absence of quadrupole admixtures leads to an $E1$ assignment for each of these transitions. As a consequence, band 4 is proposed to have negative parity.

Another new rotational band, labeled 3, has been observed and a spectrum obtained from a double gate is shown in Fig. 5(c). Bands 3 and 4 are interlinked by transitions of 321.6, 435.6 keV and 328.1, 403.7 keV, due to near degeneracies of levels between spins 8 and 14. The linking transitions indicate mixing and determine spins and parity of band 3. As seen in Fig. 5(c), the signature partner linking $\Delta I = 1$ transitions of band 3 are strong compared to the ones in bands 4 and 5.

Other new observations are a weakly populated band, labeled 2, and the fraction of a band, labeled *x*. Although coincidence relationships between these structures and prominent transitions of the level scheme are not observed, assignment of these structures to neighboring odd-A and even-even nuclei can be ruled out and assignment to ^{164}Tm is

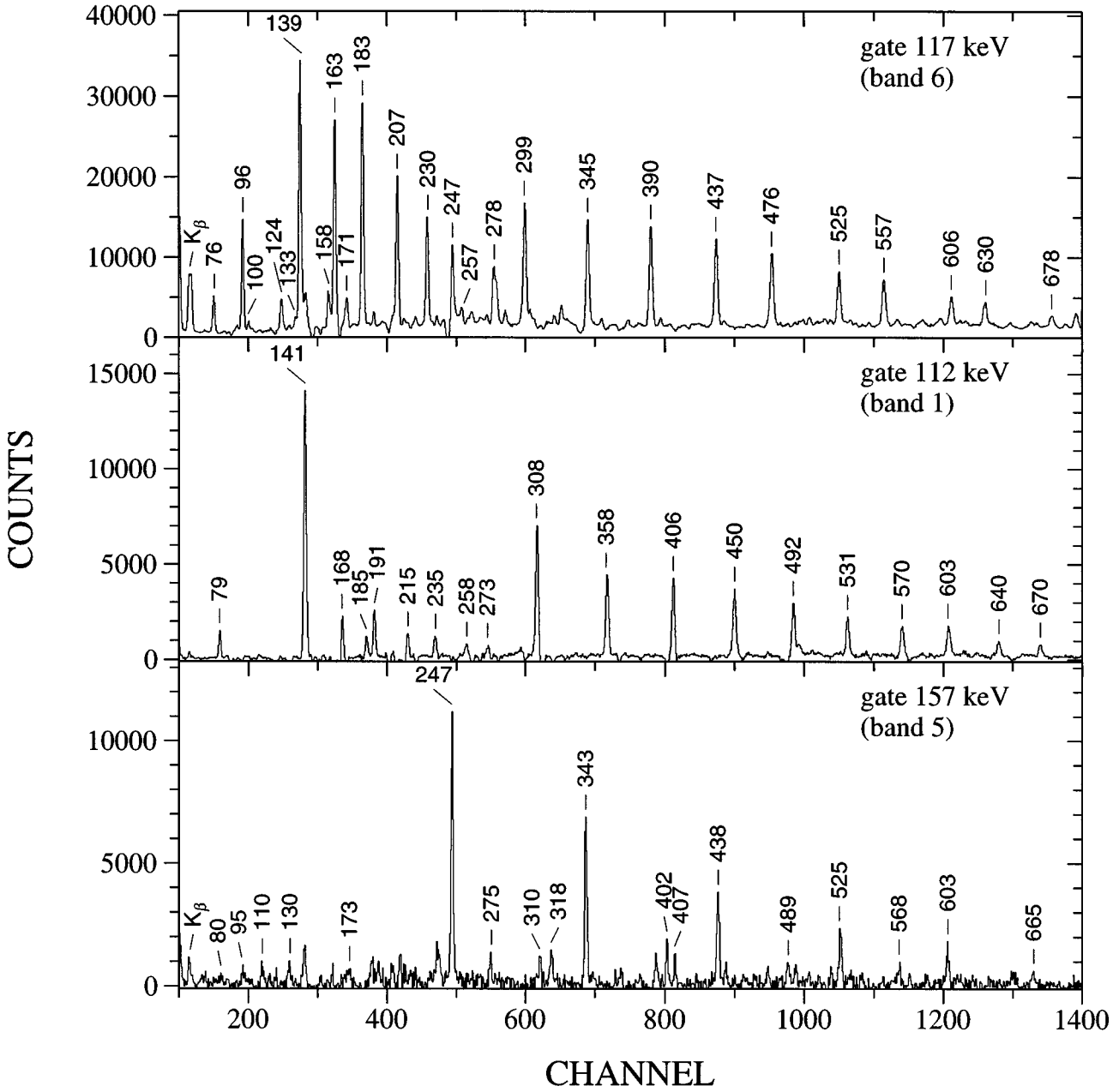

FIG. 3. Sample γ-ray spectra of ^{164}Tm for cuts on BaF_2 fold and sum energy obtained by gating on the 117 keV (top), 112 keV (mid), and 157 keV (bottom) transition. For the transitions marked with their energy, coincidences with the gated γ ray have been established. Weak contaminant peaks in the bottom spectrum are mainly from ^{165}Tm.

most likely. For the same reason, we are less confident with spin and parity assignments than for the other bands, and these quantum numbers are given in parentheses.

As a summary of our experimental findings, the excitation energies of the bands relative to a rigid rotor and their corresponding intensity patterns are plotted in Fig. 6. The close association between lower excitation energies and larger population intensities lends confidence to our spin assignments. Interesting is the comparison between the intensities for bands 4 and 5, indicating that band 4 approaches the yrast-line with increasing spin.

IV. BAND ASSIGNMENTS AND PROPERTIES

A total of nine strongly coupled rotational bands have been assigned to ^{164}Tm from the experiments described in this paper. Normally studies of odd-odd deformed nuclei are plagued by two general shortcomings, i.e., the difficulty of making connections of the bands to the known ground or isomeric state of the nucleus and the firm assignment of quasiparticle configurations to the structures observed. The first of these common difficulties was overcome in this work, with the result that almost all of the bands have proposed connections to the known ground and isomeric states in

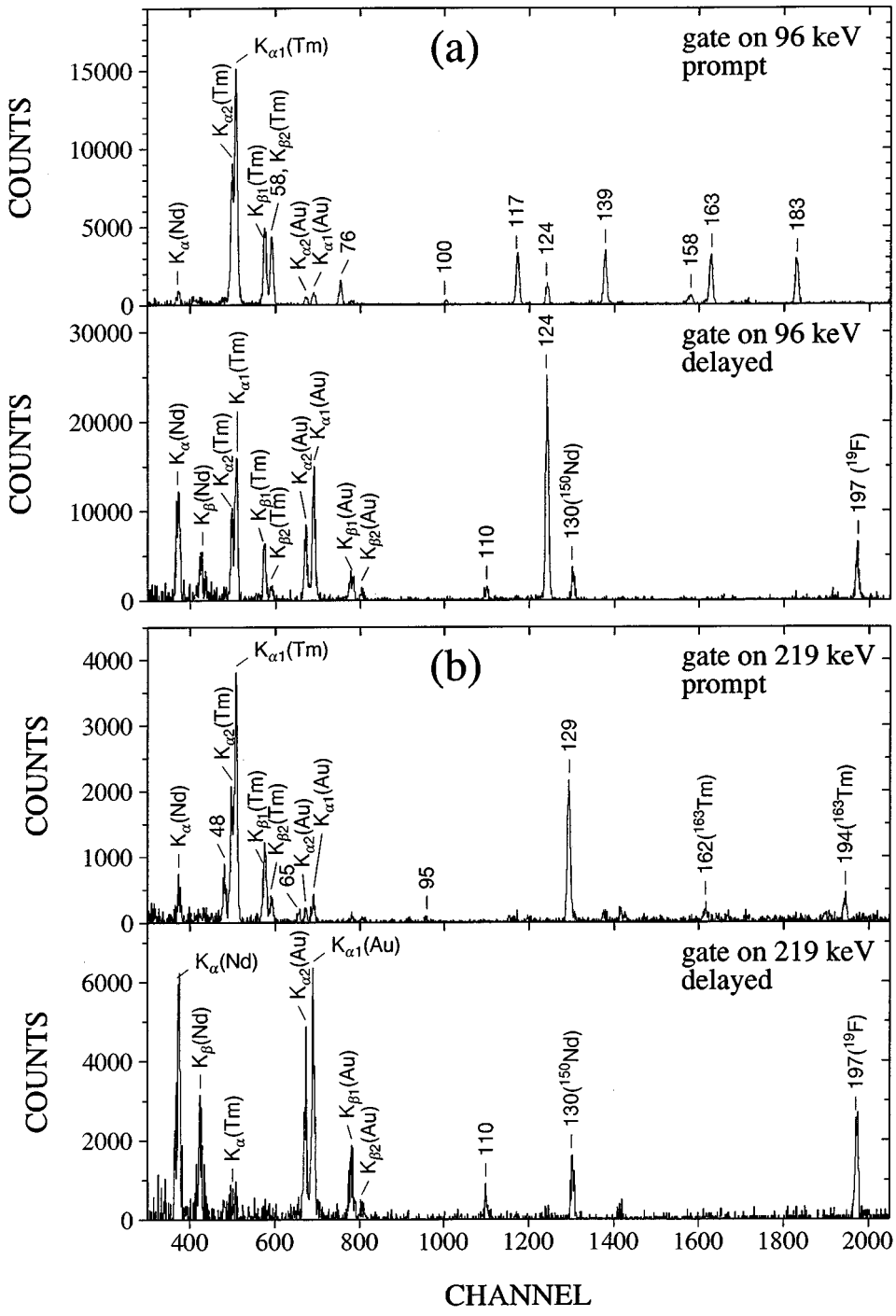

FIG. 4. Representative LEPS spectra obtained in the run using a ^{150}Nd target with Au backing: (a) gates on a prominent transition in band 6 and projections of prompt and delayed γ rays; (b) gates on a prominent transition in band 5 and projections of prompt and delayed γ rays. Peaks from random coincidences with γ decays in ^{150}Nd and ^{19}F (Coulomb excitation) or in neighboring nuclei are identified as well.

^{164}Tm, as described in the previous section. In this section we describe the process by which quasiparticle assignments are made to each of the structures, based on the properties observed and the nature of states in neighboring nuclei.

A. Couplings

The known low-lying single-particle states in the odd-A nuclei adjacent to ^{164}Tm are listed in Table II. In ^{163}Tm the five lowest bands are based on the $d_{3/2}$, $g_{7/2}$, $h_{11/2}$, and $h_{9/2}$ proton orbitals [22]. The observed energy signature splitting and quasiparticle alignment at $\hbar\omega = 0.20$ MeV for these bands are also shown in Table II, along with the known value of g_K (which indicates the $M1$ strength in each band). In ^{163}Er the lowest three single-neutron states are $h_{9/2}$, $i_{13/2}$, and $f_{7/2}$ in nature [3]. Most of the expected couplings of these five proton orbitals with the three neutron states are shown in Table III. In each case, there are two ways to

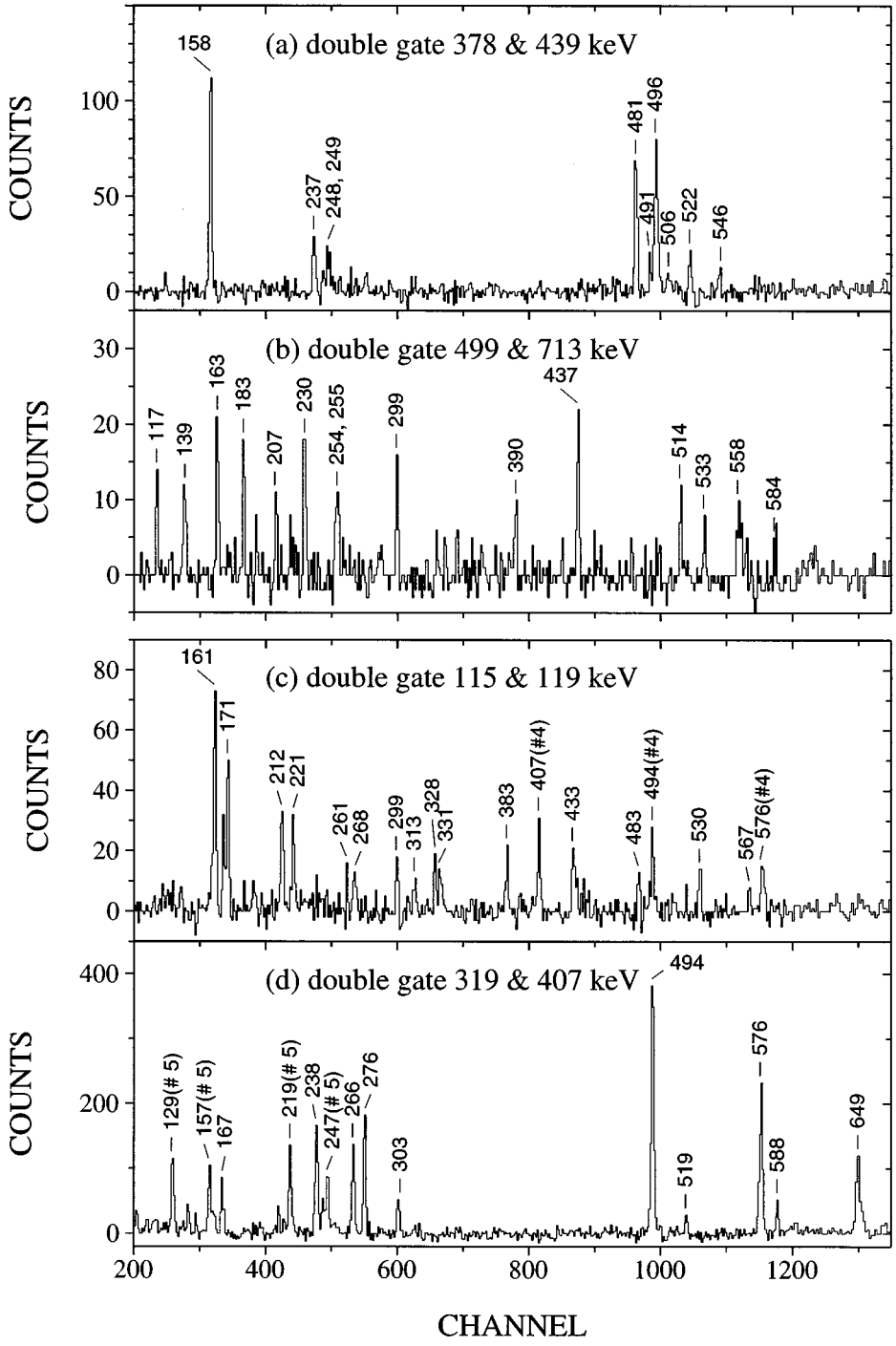

FIG. 5. Representative spectra obtained from the triples analysis: double gates on transitions in (a) band 7, (b) band 8, (c) band 3, and (d) band 4. The presence of band 4 transitions in spectrum (c) is due to the interaction between bands 3 and 4 (see text).

couple the proton and neutron states, with intrinsic spins parallel (↑↑) and antiparallel (↑↓). The Gallagher-Moszkowski rules [23] specify that in an odd-odd nucleus the parallel coupling lies lower than the antiparallel (at the band head), with the splitting in the range of 50 to 200 keV. Table III lists the K value of the two couplings in each case.

Some of the observed properties of the nine band structures are summarized in Table IV, including the observed energy signature splitting at $\hbar\omega = 0.2$ MeV, an average of the measured $B(M1)/B(E2)$ values throughout the structure, and the presence or absence of the normal alignment of $i_{13/2}$ neutrons around a frequency of 0.25 MeV (the commonly observed first backbend throughout this region). This last property can be easily observed in the standard plot of quasiparticle alignment versus frequency for the nine bands in Fig. 7. Note that the first $\nu i_{13/2}$ crossing (called the AB crossing) is clearly seen in only two bands (7 and 8), is blocked in six (1, 2, 3, 4, 5, 6), and cannot be judged in the other band (9). This immediately indicates that the $i_{13/2}$ neutron (5/2[642]) must be one of the active orbitals in bands 1

through 6, and not involved in bands 7 and 8. The crossing frequency for bands 7 and 8 is 0.23 MeV/$\hbar$, which is lower than the average of the $N=94$ and 96 Er and Yb nuclei around ^{164}Tm, 0.27 MeV/$\hbar$. This lowering is due at least partially to the well-known reduction in the neutron pairing correlations caused by blocking of the excited neutron orbital, an effect seen earlier in many odd-A nuclei [24]. It is reasonable that bands 7 and 8 would involve the lowest neutron orbital in ^{163}Er, 5/2[523]. Many of the bands with the AB crossing blocked show full or partial evidence for a delayed $\nu i_{13/2}$ crossing (BC) at a frequency around 0.35 MeV/$\hbar$.

The assignment of the proton orbital involved in the ^{164}Tm bands is also straightforward in most cases. The $h_{11/2}$ proton orbital has the largest g_K factor in the odd-Z nuclei (see Table II), and so it seems clear that bands 3 and 6 must involve this orbital, since they have the largest observed $B(M1)/B(E2)$ values (see Table IV). Band 6 is the most strongly populated structure and lies lowest in energy (see Fig. 6), so it is logical that it should involve the low-lying proton orbital $\pi h_{11/2}$ (which becomes yrast with frequency in ^{163}Tm). It is also clear that this would be the high-K coupling of $\pi h_{11/2}\nu i_{13/2}$, since the Gallagher-Moszkowski rules place the $K=6(\uparrow\uparrow)$ coupling lower in energy than the $K=1\uparrow\downarrow$ band, to which we assign band 3. This $K=1$ assignment for band 3 is also logical in view of its interaction with band 4 that we also assign to a low-K quasiparticle configuration (see below).

Band 1 is the second most strongly populated and lowest lying band, and so it is logical that it should involve the $g_{7/2}$ proton orbital (7/2[404]). Its low $B(M1)/B(E2)$ value and its blocked AB crossing lead to the assignment of $\pi g_{7/2}\nu i_{13/2}$. The $K=6$ coupling of this configuration is assigned, partially in agreement with tilted cranking calculations described in Sec. V and also since these two $K=6$ bands (the equivalents of our bands 1 and 6) are seen throughout the odd-odd nuclei in this region. We assign band 2 to the low-K coupling of $\pi g_{7/2}\nu i_{13/2}$, in view of its small signature splitting, low $B(M1)/B(E2)$ value, and blocked AB crossing.

The observed values of energy signature splitting can also be understood in terms of the involved quasiparticle orbitals. As seen in Table II, the $\pi h_{11/2}$ and $\pi g_{7/2}$ bands have no signature splitting in ^{163}Tm, since both have $K=\frac{7}{2}$ and are deformation aligned. Bands resulting from the coupling of these two orbitals to $\nu i_{13/2}$ ($\uparrow\uparrow$ and $\uparrow\downarrow$) naturally have no signature splitting, since the $\nu i_{13/2}$ orbital in ^{163}Er has large splitting (160 keV—see Table II). That is, in the terminology of the cranked shell model, signature A of $\nu i_{13/2}$ couples with the two very close lying signatures of $\pi h_{11/2}$ (or $\pi g_{7/2}$) to form a band with no signature splitting, while the higher lying signature B of $\nu i_{13/2}$ also couples with the same proton orbital to form another band of no splitting. These two correspond to the $\uparrow\uparrow$ and $\uparrow\downarrow$ couplings of the two orbitals, $7/2[523]_\pi$ and $5/2[642]_\nu$. So, the absence of signature splitting for bands 1, 2, 3, and 6 is reasonable in view of the quasiparticle assignments listed in Tables III and IV.

The $d_{3/2}$ 1/2[411] orbital is the ground state of ^{163}Tm (see Table II) and must certainly be involved in the spectrum of bands in ^{164}Tm. It has large signature splitting (but smaller than that of $\nu i_{13/2}$) and so its coupling with the expected $\nu i_{13/2}$ orbital should produce a band with splitting. Bands 4 and 5 both have signature splitting, are low lying, and have blocked $\nu i_{13/2}$ crossings. The fact that band 5 lies lower than band 4 (see Fig. 6) is one reason for the assignment of this to the $\pi d_{3/2}\nu i_{13/2}$ configuration. The other proton orbital expected is $\pi h_{9/2}$ 1/2[541], which has very large signature splitting and lies somewhat high at the band head but gains alignment and comes lower in energy (even yrast) at higher frequency. We assign band 4 to the $\pi h_{9/2}\nu i_{13/2}$ configuration. This assignment is also consistent with the observation of interlinking transitions between bands 3 and 4 indicating that both structures have the same parity. The interaction strength deduced is on average $\sim$5 keV, which is in agreement with corresponding band crossings in ^{163,165}Tm [22,25].

Band 7 seems to be in the high-K part of the level scheme (built on the $I=6$ isomer), since there is a transition connecting bands 6 and 7. Since the $\nu i_{13/2}$ AB crossing occurs in band 7 (see Fig. 7), the neutron configuration must be something besides $i_{13/2}$, and the lowest one seen in ^{163}Er is 5/2[523] ($h_{9/2}$). Concerning the involved proton orbital, the low $B(M1)/B(E2)$ value leads us to choose $g_{7/2}$ rather than $h_{11/2}$, leading to a $\pi g_{7/2}\nu h_{9/2}$ assignment. Band 8 is seen only after the $\nu i_{13/2}$ bandcrossing at $\hbar\omega=0.23$ MeV (very similar to the crossing seen in full fashion in band 7), and decays by dipole transitions to the $K=6^+$ band 6 just above the band crossing in band 8. It seems likely that the active neutron orbital for band 8 is the same as that of band 7 (5/2[523]). The large $B(M1)/B(E2)$ value for band 8 indicates that the $\pi h_{11/2}$ orbital is involved, leading to a $\pi h_{11/2}\nu h_{9/2}(\nu i_{13/2})^2$ assignment. The pattern of decays from band 8 to band 6 ($\pi h_{11/2}\nu i_{13/2}$) is very similar to that seen in ^{163}Er, where the $\nu h_{9/2}$ band decays by a number of dipole transitions to the yrast $\nu i_{13/2}$ band.

Band 9 is difficult to assign with certainty. It must have a high value of K since it decays to the $K=6$ band 1. Looking at the available configurations in Table III, one concludes that band 9 could be a $K=5$ $7/2[523]_\pi 3/2[521]_\nu$ or $7/2[404]_\pi 3/2[521]_\nu$ configuration. We choose the former in view of the size of $B(M1)/B(E2)$ for this band.

B. Additivity of Routhians

Table IV lists the quasiparticle assignments for all nine bands observed, based on the measured properties of the structures. It is important now to learn if the nine bands have excitation energies that are reasonable, in view of the ordering of the single-particle levels in the adjacent odd-A nuclei (e.g., in Table II). One can sometimes do this analysis of band positions at the band heads, incorporating the systematically occurring Gallagher-Moszkowski splitting between the parallel and antiparallel couplings [23]. But, the problem in high-spin spectroscopy is that bands are populated from above and sometimes lose population intensity before the band head is reached. That is the case here, and so an analysis of intrinsic states is impossible.

It is only possible to do the analysis of the energetics of the nine bands in ^{164}Tm in the rotating frame of the nucleus. In the usual manner, the Routhian for the rotational band is defined as

$$e'(\omega)=E'(\omega)-E'_{\rm ref}(\omega), \tag{4.1}$$

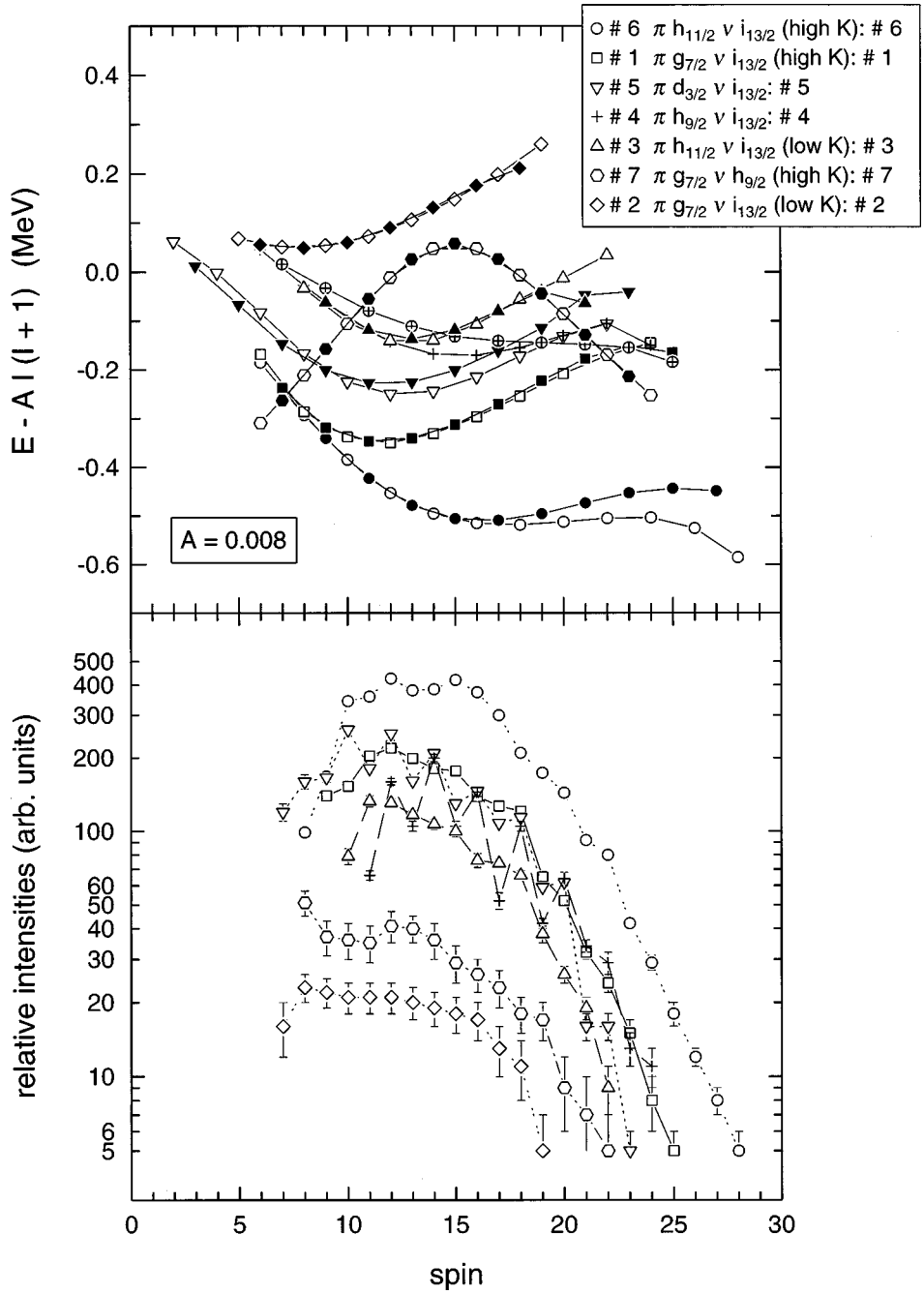

FIG. 6. Top: Experimental excitation energies versus spin relative to a rigid rotor. Bottom: Population strength of the bands in ^{164}Tm. Plotted are the summed intensities in all decay branches from a given spin. The intensities of the transitions are corrected for internal conversion.

where $E'=E-\hbar\omega I_x$, $\hbar\omega=dE/dI_x$ and the reference energy in a Harris description is

$$E'_{\mathrm{ref}}=-\frac{1}{2}\omega^2\mathcal{J}_0-\frac{1}{4}\omega^4\mathcal{J}_1+\frac{1}{8\mathcal{J}_0}. \tag{4.2}$$

Similarly, the aligned angular momentum is defined as

$$i(\omega)=I_x(\omega)-I_{\mathrm{ref}}(\omega), \tag{4.3}$$

where the reference angular momentum is $I_{\mathrm{ref}}=dE'_{\mathrm{ref}}/d\omega$. As Harris parameters, $\mathcal{J}_0=35\hbar^2/\mathrm{MeV}$ and $\mathcal{J}_1=40\hbar^4/\mathrm{MeV}^3$ are chosen.

The Routhians (energies in the rotating frame) for the nine band structures in ^{164}Tm are shown in Fig. 8. As discussed earlier by Frauendorf *et al.* [26], it is possible to compare these Routhians with the sums of the Routhians for the measured one-quasiparticle bands in the adjacent odd-*A* nuclei. This provides a rotating-frame analysis of the additivity of the one-quasiparticle bands to form the two-quasiparticle bands seen in odd-odd ^{164}Tm. To perform this analysis, we extract from measured bands in ^{163}Tm [22] and ^{163}Er [3] the Routhians at one rotational frequency ($\hbar\omega=0.20$ MeV), add them, and compare to the measured Routhians for the various bands in ^{164}Tm (at the same rotational frequency).

The results of this analysis are shown in Table V for

TABLE II. Single-proton and single-neutron states in neighboring nuclei of ^{164}Tm. The g_K values are taken from a compilation in Bohr and Mottelson [42] if not referenced. The other three parameters are extracted from the level schemes of ^{163}Tm [22] and ^{163}Er [3].

Orbital	g_K	E_x (keV)	$\Delta e'$ (keV)	i ($\hbar$)
^{163}Tm (protons)				
$1/2[411]d_{3/2}$	−1.57	0	100	0.1
$7/2[404]g_{7/2}$	0.73	23	0	0.1
$7/2[523]h_{11/2}$	1.35	87	0	1.4
$5/2[402]d_{5/2}$		136	0	0.1
$1/2[541]h_{9/2}$		248	470	2.5
^{163}Er (neutrons)				
$5/2[523]h_{9/2}$	0.20[a]	0	8	2.2
$5/2[642]i_{13/2}$	−0.34	69	160	4.5
$3/2[521]f_{7/2}$	−0.50	104		1.0
$11/2[505]h_{11/2}$		444	0	

[a]From Ref. [43].

bands 6, 1 (assuming $E=30$ keV for the 6^- isomer) and bands 3–5. (Bands 7 and 8 are not analyzed in this way since the band crossing could affect the cleanliness of this additivity, while band 2 is excluded since its band head energy is not known.) It is striking that the Routhians for bands 6, 1, and 3 lie within 50 keV (for the latter at most 100 keV considering the uncertainty of the linking transition between the low-K bands and the ground state) of where they should be, based on summing the Routhians of the component quasiparticles. In the terminology of Frauendorf *et al.* [26], this difference is a residual interaction, i.e., effects not included in the mean field of the nucleus. Small variations in deformation (and other field variables) certainly contribute to differences of this order. And, the values of V_{ij} listed in Table V are only slightly dependent on the Harris parameters chosen for the rotating reference. Increasing $\mathcal{J}_1$ from 40 to 80 $\hbar^4$/MeV^3 would decrease V_{ij} by at most 10 keV.

It is interesting that the good agreement between observed versus summed energies holds for both the parallel and antiparallel couplings of $\pi h_{11/2}\nu i_{13/2}$ and $\pi g_{7/2}\nu i_{13/2}$. This analysis includes no Gallagher-Moszkowski shift between the $\uparrow\uparrow$ and $\uparrow\downarrow$ band heads, but rather the differences that result in the last column of Table V can be viewed as containing this effect (which results from a proton-neutron spin residual interaction), in addition to other residual effects such as small differences in deformations and pairing parameters and changes in the angle of rotation (to be discussed in Sec. V).

The additivity of Routhians for band 4 is an interesting case. The even-spin signature ($\alpha=0$) of band 4 has perfect agreement between its energy and the sum of the components. But, the odd spins have the largest observed shift, such that this signature lies 230 keV too high in the rotating frame. This substantial increase even gives rise to an inversion in the signatures, which is discussed in Sec. VI in terms of the particle-rotor model. We find that the inclusion of a residual proton-neutron interaction has the effect of inverting the signatures in this $\pi h_{9/2}\nu i_{13/2}$ band, and not in other configurations. It is interesting here in the Routhian analysis that this inversion of signature seems to be primarily the result of the odd spins being pushed substantially up in energy.

TABLE III. Expected configurations in odd-odd ^{164}Tm and proposed assignments to the bands observed. Left columns: known proton and neutron levels in neighboring odd-A nuclei labeled by their Nilsson quantum numbers and a symbol for ''spin up'' or ''spin down.'' Right columns: doublets of couplings for parallel and antiparallel proton and neutron spins labeled by the $K=K_p\pm K_n$ value. In parentheses, the number of the observed band is given.

Orbitals		Couplings odd-odd K^π	
p	n	lower $\uparrow\uparrow$	higher $\uparrow\downarrow$
$7/2[523]\uparrow$	$5/2[523]\downarrow$	1^+ (g.s.)	6^+ (8)
$7/2[404]\downarrow$	$5/2[523]\downarrow$	6^- (isomer, 7)	1^-
$1/2[411]\downarrow$	$5/2[523]\downarrow$	3^-	2^-
$5/2[402]\uparrow$	$5/2[523]\downarrow$	0^-	5^-
$1/2[541]\downarrow$	$5/2[523]\downarrow$	3^+	2^+
$7/2[523]\uparrow$	$5/2[642]\uparrow$	6^- (6)	1^- (3)
$7/2[404]\downarrow$	$5/2[642]\uparrow$	1^+ (2)	6^+ (1)
$1/2[411]\downarrow$	$5/2[642]\uparrow$	2^+ (5)	3^+
$5/2[402]\uparrow$	$5/2[642]\uparrow$	5^+	0^+
$1/2[541]\downarrow$	$5/2[642]\uparrow$	2^- (4)	3^-
$7/2[523]\uparrow$	$3/2[521]\uparrow$	5^+ (9)	2^+
$7/2[404]\downarrow$	$3/2[521]\uparrow$	2^-	5^-

C. Shift of crossing frequency

The fact that the $\alpha=1$ signature of the $\pi h_{9/2}\nu i_{13/2}$ band lies 230 keV too high in energy (at $\hbar\omega=0.2$ MeV) compared to the sum of the component Routhians (see the previous section) is related to a long-standing problem of delayed $\nu i_{13/2}$ crossing frequencies in the $\pi h_{9/2}$ bands in odd-A nuclei in this region. As discussed by Jensen *et al.* [27,25], it is a common problem that the standard $\nu i_{13/2}$ crossing in the $\pi h_{9/2}$ band is delayed by up to 80 keV compared to the

TABLE IV. Properties of the nine measured bands in ^{164}Tm: signature splitting, average $B(M1;I\to I-1)/B(E2;I\to I-2)$ value, occurrence of the $\nu i_{13/2}$ (AB) band crossing, assigned K value, and configuration.

Band	$\Delta e'$[a] (keV)	Average $B(M1)/B(E2)$ (μ^2/e^2 b^2)	$\nu i_{13/2}$ crossing[b]	K	Assigned configuration
1	2	0.2	no	6	$\pi g_{7/2}\nu i_{13/2}$ ($\uparrow\downarrow$)
2	2	0.1	no	1	$\pi g_{7/2}\nu i_{13/2}$ ($\uparrow\uparrow$)
3	7	1.3	no	1	$\pi h_{11/2}\nu i_{13/2}$ ($\uparrow\downarrow$)
4	49	0.3	no	2	$\pi h_{9/2}\nu i_{13/2}$ ($\uparrow\uparrow$)
5	19	0.1	no	2	$\pi d_{3/2}\nu i_{13/2}$ ($\uparrow\uparrow$)
6	2	0.9	no	6	$\pi h_{11/2}\nu i_{13/2}$ ($\uparrow\uparrow$)
7	1	0.5	yes	6	$\pi g_{7/2}\nu h_{9/2}$ ($\uparrow\uparrow$)
8		1.2[c]	yes	6	$\pi h_{11/2}\nu h_{9/2}$ ($\uparrow\downarrow$)
9	9	0.9		5	$\pi h_{11/2}\nu f_{7/2}$ ($\uparrow\uparrow$)

[a]Extracted at $\hbar\omega=0.20$ MeV.
[b]At $\hbar\omega\sim0.25$ MeV.
[c]After the $\nu i_{13/2}$ crossing.

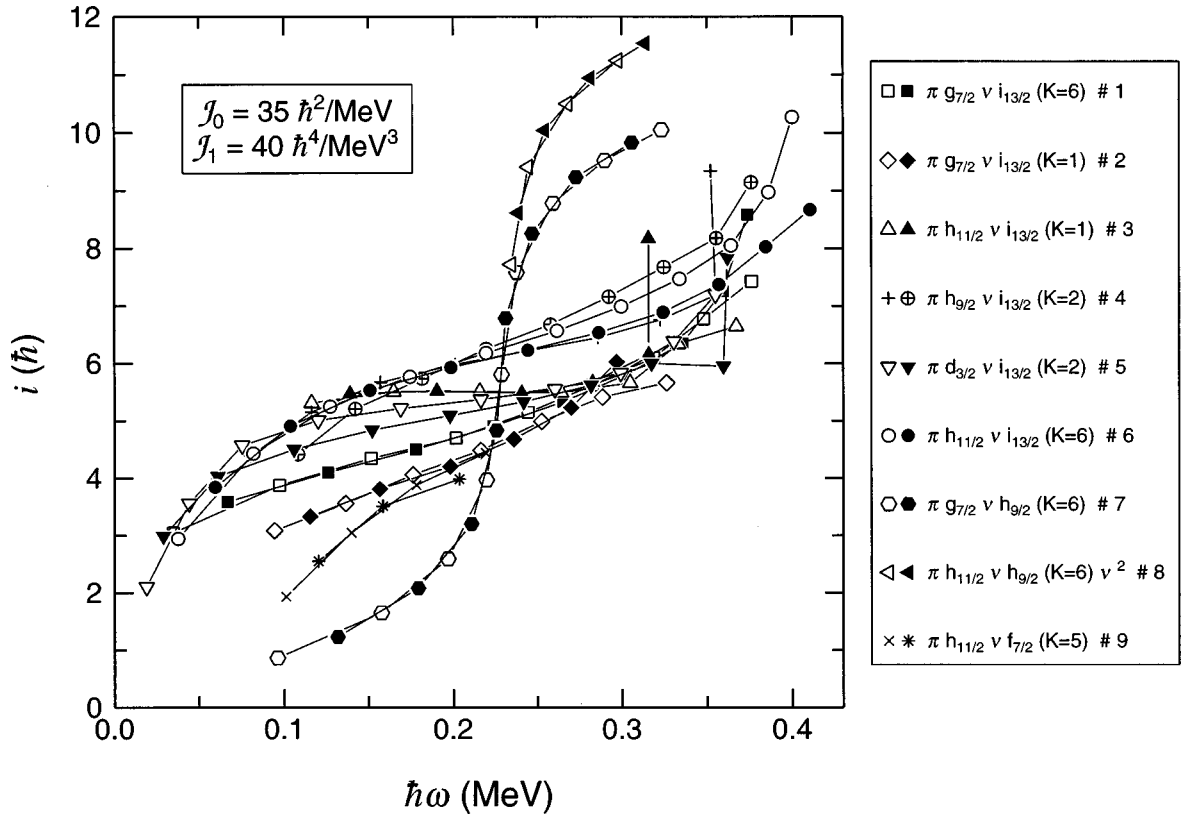

FIG. 7. Aligned angular momenta versus rotational frequency for the nine rotational bands assigned to ^{164}Tm. The K values assigned to these bands (see Tables III or IV) are used to calculate the values. The rotating reference is described by the parameters $\mathcal{J}_0 = 35\hbar^2\,\mathrm{MeV}^{-1}$ and $\mathcal{J}_1 = 40\hbar^4\,\mathrm{MeV}^{-3}$. The first symbol displayed in the legend for each band refers to the $\alpha = 0$ signature.

values in other bands in the same odd-A nucleus or in adjacent even-even nuclei. This delay is 70–80 keV in ^{163}Tm and ^{165}Tm [22,25]. The relationship between the selective upward shift of the odd-spin $\pi h_{9/2}\nu i_{13/2}$ Routhian and the $\nu i_{13/2}$ crossing frequency in odd-A nuclei is shown below. To aid this derivation, we define in Table VI the relevant quasiparticles by letters, and show in Table V the association of the Routhian shifts with residual interactions $V_{i,j}$ between these various orbits.

As shown in the schematic Fig. 9, the $\nu i_{13/2}$ crossing in the $\pi h_{9/2}$ band is denoted by the intersection of the one-quasiparticle Routhian g with a three-quasiparticle Routhian gAB at a certain rotational frequency, $\hbar\omega_c$. The actual crossing between g and gAB is shifted to a higher frequency than expected for unperturbed Routhians (denoted by the u), since the Routhian gAB is shifted up in energy by the p-n interaction, $V_{pn} = V_{gA} + V_{gB}$.

The Routhians for the relevant configurations can be written as

$$e_g(\omega) = e_g^0 - i_g \cdot \omega, \tag{4.4}$$

$$e_{uAB}(\omega) = e_{uAB}^0 - i_{uAB} \cdot \omega, \tag{4.5}$$

$$e_{gAB}(\omega) = (e_{uAB}^0 + V_{pn}) - i_{gAB} \cdot \omega. \tag{4.6}$$

From this one can express the frequency for the crossing of g with the unperturbed configuration uAB and with the perturbed configuration gAB as

$$\hbar\omega_c^u = \frac{e_{uAB}^0 - e_u^0}{i_{uAB}^0 - i_u^0} \quad \text{and} \quad \hbar\omega_c^g = \frac{e_{uAB}^0 + V_{pn} - e_g^0}{i_{gAB}^0 - i_g^0}. \tag{4.7}$$

The shift in crossing frequency can consequently be expressed by

$$\delta\hbar\omega_c = \hbar\omega_c^g - \hbar\omega_c^u \approx \frac{(e_{uAB}^0 + V_{pn} - e_g^0) - (e_{uAB}^0 - e_u^0)}{\Delta i_g} = \frac{V_{pn}}{\Delta i_g}. \tag{4.8}$$

If the gain in alignment in the crossing is the same in the unperturbed and perturbed cases ($\Delta i_g \approx \Delta i_u$), then

$$\delta\hbar\omega_c = \frac{V_{gA} + V_{gB}}{\Delta i_g}. \tag{4.9}$$

Experimentally we get $V_{gA} + V_{gB} \approx 230$ keV (see Table V) and $\Delta i_g \approx 7\hbar$ (see the alignment gain in band 7 in Fig. 7), which gives $\delta\hbar\omega_c \approx 35$ keV. This represents about half of the total delay seen experimentally in ^{163}Tm and ^{165}Tm. As discussed by Jensen *et al.* [27,25], cranked shell model calculations have generally been able to explain about half of this frequency delay as a result of the known increase in deformation in the $\pi h_{9/2}$ configuration. But, from the present data and analysis, it seems that one can attribute the other half of the delay in the $\nu i_{13/2}$ crossing in $\pi h_{9/2}$ bands to a residual p-n interaction. A similar conclusion has been reached in recent work on ^{174}Ta [9].

D. Signature splitting

The energy splitting between signatures of a rotational band is an important quantity for judging the nature of the configuration, as was discussed in Sec. IV A. The splittings in the nine bands of ^{164}Tm can be seen from the Routhians plotted in Fig. 8. Most bands have essentially no signature splitting, as is compiled in the second column of Table IV. This is because most bands (1, 2, 3, 6, 7) involve the coupling of proton orbitals ($h_{11/2}$ and $g_{7/2}$) which have high K ($\frac{7}{2}$) and small signature splitting with a neutron orbital of nonzero splitting ($i_{13/2}-160$ keV; $h_{9/2}-8$ keV, at $\hbar\omega=0.2$ MeV; see Table II), resulting in an odd-odd band that reflects the essentially zero signature splitting of the proton orbital.

The only structures with significant splitting are bands 4 and 5 (see Table IV). The signature splitting of the latter structure ($\pi d_{3/2}\nu i_{13/2}$) is 19 keV at $\hbar\omega=0.2$ MeV, which is much smaller than the splitting of the 1/2[411] band in ^{163}Tm (100 keV) and ^{165}Tm (116 keV) or of the $\nu i_{13/2}$ band in ^{163}Er (160 keV). Band 4 is assigned to $\pi h_{9/2}\nu i_{13/2}$. The $\alpha=+\frac{1}{2}$ signature is favored (i.e., low in energy) for both component quasiparticles, so the $\alpha=1$ (odd-spin) signature should be lower in energy than $\alpha=0$ (even spins) for band 4. This is the case for rotational frequency above 0.3 MeV, but below this point the $\alpha=0$ trace is lower in energy, giving an inversion in signature (see Fig. 8).

The signature properties of the bands can be studied more carefully by comparing the energy of a given level with the average of the energies of the signature-partner levels with one unit of spin higher and lower. This ''staggering'' function is plotted in Fig. 10 for bands 6 and 3 ($\pi h_{11/2}\nu i_{13/2}$), 4 ($\pi h_{9/2}\nu i_{13/2}$), and 5 ($\pi d_{3/2}\nu i_{13/2}$) in ^{164}Tm. Note that band 6 has essentially no signature staggering until $I=16$ when the expected $\alpha=0$ component comes lower (note that the more negative value of the staggering function means that this particular signature is lower in energy and thus favored). There is significant inversion of signature in the $\pi h_{11/2}\nu i_{13/2}$ bands for $N=89$ nuclei [28], but the size of this inversion decreases with increasing N, to the point where there is no inversion for ^{164}Tm. It is interesting that there is a small staggering in band 3, the $\uparrow\downarrow$ coupling of $\pi h_{11/2}\nu i_{13/2}$, with even spins low over most of the band. This represents a small signature inversion up to $I=18$, where the expected lower-lying $\alpha=1$ (odd-spin) signature (see Sec. IV A) becomes favored.

Band 5 has a signature inversion up to $I=8\hbar$, above which the expected $\alpha=0$ component becomes favored. Kreiner and Mariscotti [29] and Hamamoto [30] have discussed the possibility that inversions can occur when $I<j_p+j_n$, since the angular momentum couplings are complicated in this regime. However, those arguments were made for high-j configurations, where j_p and j_n are approximately good quantum numbers. The 1/2[411] Nilsson orbital, although mainly built from the $d_{3/2}$ spherical orbital ($\sim$55%), also has significant contributions ($>$10%) from the $d_{5/2}$, $g_{7/2}$, and $s_{1/2}$ orbitals. Consequently, the signature inversion in band 5 is somewhat surprising.

The largest signature inversion is found in band 4, $\pi h_{9/2}\nu i_{13/2}$. This band is expected to have $\alpha=1$ favored, but this does not occur until $I=20\hbar$ and above. It is striking that the persistent (but decreasing with N) inversion in the yrast $\pi h_{11/2}\nu i_{13/2}$ band is replaced here by a large inversion in the $\pi h_{9/2}\nu i_{13/2}$ structure. As discussed in Sec. IV B, this inversion seems to result from a 230 keV upward shift of the $\alpha=1$ Routhian relative to $\alpha=0$. An explanation for the selective appearance of this inversion was outlined in an earlier letter [10] and is discussed in more detail in Sec. VI.

V. TILTED CRANKING

While models based on cranking about the principal (1) axis of the nucleus have had remarkable success in explaining the properties of deformed nuclei, there are certain situations where this approach of principal-axis cranking (PAC) is not adequate. Brockstedt *et al.* [3] illustrated the success of the model of tilted axis cranking (TAC) in explaining various features of ^{163}Er, the isotone of ^{164}Tm, including the existence of low-lying bands of high K, specifically two $K=\frac{19}{2}$ sequences based on $\pi h_{11/2}\pi g_{7/2}$ (each $K=\frac{7}{2}$) coupled to the $K=\frac{5}{2}$ $\nu i_{13/2}$ and $\nu h_{9/2}$ orbitals. Significant angles of tilt develop for these high-K bands. For the $K=\frac{19}{2}^+$ band the angular momentum of the 7/2[404] lies mostly along the three axis (since it is the orbital with $\Omega=j=\frac{7}{2}$), the $\frac{7}{2}$[523] angular momentum is also mostly aligned with the three axis, but the $\frac{5}{2}$[642] angular momentum is more closely aligned along the rotation axis (one axis) of the nucleus. At a low rotational frequency ($\hbar\omega=0.15$ MeV), the resulting angle of the total angular momentum is $\theta=45°$, quite an excursion from the assumption of PAC. Of course, the tilt angle increases towards 90° (principal-axis cranking) with increasing rotational frequency, due to the addition of collective angular momentum along the one axis. But, it is clear that the low to medium spin properties of these high-K bands depend critically on this rather extreme angle of tilt.

It is interesting to see how this concept of tilted-axis cranking affects the properties of the observed ^{164}Tm bands, which involve two of the three quasiparticles which comprise the tilted structures in ^{163}Er. Of the nine structures observed in ^{164}Tm, seven have no significant signature splitting, indicating that these are candidates for bands with tilted cranking. In this section we describe TAC calculations for these various bands, compare the results to measurements of K, spin, and $B(M1)/B(E2)$, and demonstrate that $\theta\neq 90°$ is present and required to explain these observables. In addition, the TAC calculations can explain the observed crossing frequency for band 7, $\pi g_{7/2}\nu h_{9/2}$.

A. Multiband spectrum of ^{164}Tm in the TAC scheme

Tilted cranking calculations have been performed following the Frauendorf [4] prescription applied in detail by Brockstedt *et al.* [3] to measured bands in ^{163}Er. In our calculations on ^{164}Tm, standard pair-gap parameters $\Delta_p=0.86$ and $\Delta_n=0.88$ MeV have been used, along with deformation parameters $\epsilon_2=0.247$ (consistent with measured Q_0 values in neighboring Er nuclei), $\epsilon_4=-0.002$, and $\gamma=0°$. The results of the calculations for the 19 lowest configurations are shown in Table VII at a rotational frequency of $\hbar\omega=0.20$ MeV. Listed here for each configuration is the calculated value of the angular momentum along the one and three axes (where I_3 would correspond to the well-known K value

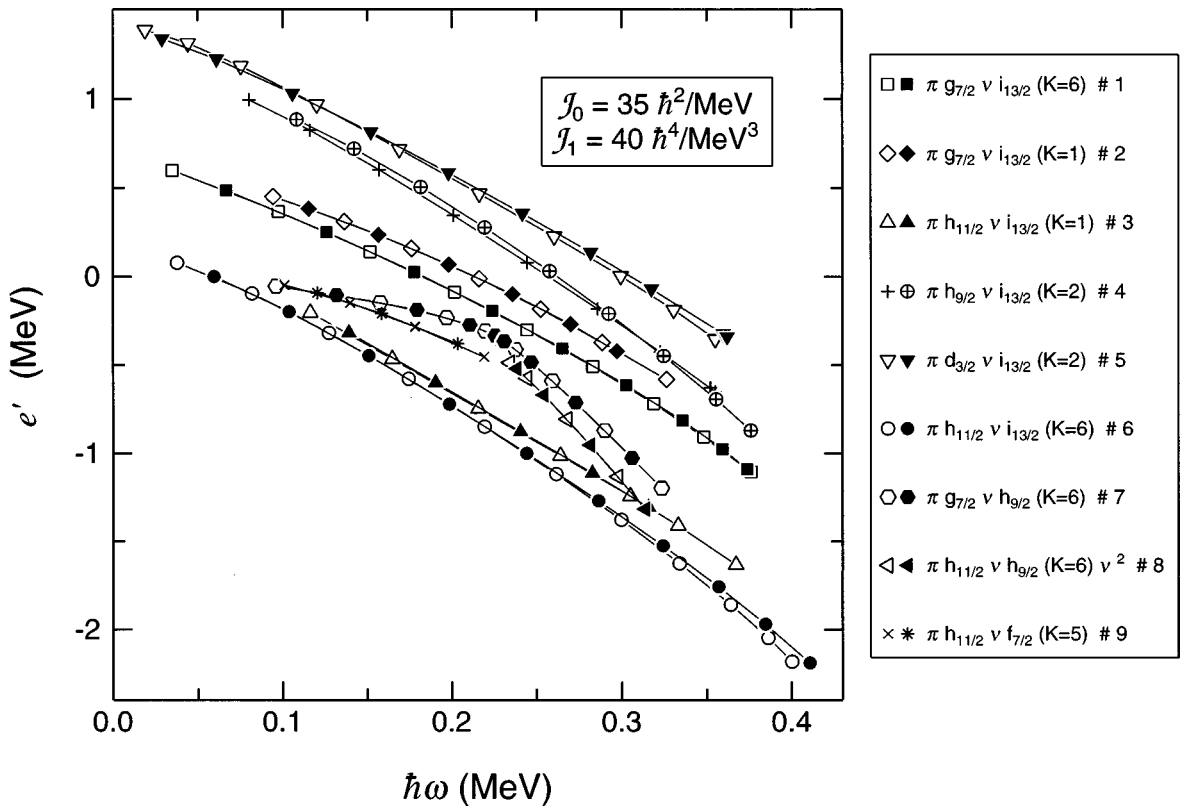

FIG. 8. Routhians versus rotational frequency for the nine rotational bands assigned to ^{164}Tm. The K values assigned to these bands (see Tables III or IV) are used to calculate the values. The rotating reference is described by the parameters $\mathcal{J}_0 = 35\hbar^2\,\mathrm{MeV}^{-1}$ and $\mathcal{J}_1 = 40\hbar^4\,\mathrm{MeV}^{-3}$. Since all the Routhians are similar in energy, those for bands 1 and 2 are shifted up in energy by 0.5 MeV for the plot, those for band 4 by 1.0 MeV, and those for band 5 by 1.3 MeV. The first symbol displayed in the legend for each band refers to the $\alpha = 0$ signature.

of the band, and I_1 to the aligned angular momentum), in addition to the total angular momentum which results from the combination of the I_1 and I_3 values. Also shown are the calculated values of the equilibrium angle of tilt θ_{eq} of the rotation axis relative to the one axis (principal cranking axis) and the relative energy of that excitation. Table VII also includes a comparison to the measured nine bands, matching the experimental band number with the assigned quasiparticle configuration, and giving for $\hbar\omega = 0.20\,\mathrm{MeV}$ the measured band energy in the rotating frame at the same frequency (note that $K = 0$ must be used in calculating the experimental Routhian in this case, to allow a comparison to TAC results), the assigned band-head K (based on the quasiparticle couplings described in Table III), and the measured angular momentum I_{exp}. Table VII shows which bands have a tilted axis of rotation, shown by θ_{eq} diverging from 90°. Since the neutron orbits near the Fermi level have low to medium values of K, it is the proton orbitals that determine the effective angle of tilt. Some configurations (e.g., 4, 7, 8, 11, and 15) have no tilt relative to the 1 axis, since these involve the $\frac{1}{2}$[411] or $\frac{1}{2}$[541] proton states. These bands are well described by principal-axis cranking. All of the configu-

TABLE V. Comparison of measured Routhians for bands in ^{164}Tm and the sum of the proton and neutron components. These components are extracted from one-quasiparticle Routhians in ^{163}Tm [22] and ^{163}Er [3]. The last column denotes the nomenclature for residual interaction between quasiparticles i and j, which is listed numerically in the previous column. The letters are defined in Table VI.

Band	Configuration	α	e'^{a} (MeV)	$\pi e'^{\mathrm{a}}$ (MeV)	$\nu e'^{\mathrm{a}}$ (MeV)	Sum: actual (MeV)	$V_{i,j}$
6	$\pi h_{11/2}\nu i_{13/2}$ (↑↑)	0,1	−0.74	−0.14	−0.65	−0.05	*eA,fA*
3	$\pi h_{11/2}\nu i_{13/2}$ (↑↓)	0,1	−0.66	−0.14	−0.48	+0.04	*eB,fB*
1	$\pi g_{7/2}\nu i_{13/2}$ (↑↓)	0,1	−0.58	+0.02	−0.65	−0.05	*aA,bA*
5	$\pi d_{3/2}\nu i_{13/2}$ (↑↑)	1	−0.75	−0.05	−0.65	+0.05	*cA*
	$\pi d_{3/2}\nu i_{13/2}$ (↑↑)	0	−0.73	+0.05	−0.65	+0.13	*dA*
4	$\pi h_{9/2}\nu i_{13/2}$ (↑↑)	0	−0.65	−0.18	−0.48	−0.01	*gB*
	$\pi h_{9/2}\nu i_{13/2}$ (↑↑)	1	−0.60	−0.18	−0.65	−0.23	*gA*

[a]Extracted at $\hbar\omega = 0.20$ MeV.

TABLE VI. Definition of the alphabetic labeling used in Table V and in the text for the relevant proton and neutron configurations.

Protons			Neutrons		
Configuration	$\alpha=+\frac{1}{2}$	$\alpha=-\frac{1}{2}$	Configuration	$\alpha=+\frac{1}{2}$	$\alpha=-\frac{1}{2}$
$\pi g_{7/2}$ 7/2[404]	*a*	*b*	$\nu i_{13/2}$ 5/2[642]	*A*	*B*
$\pi d_{3/2}$ 1/2[411]	*c*	*d*	$\nu i_{13/2}$ 3/2[651]	*C*	*D*
$\pi h_{11/2}$ 7/2[523]	*e*	*f*	$\nu h_{9/2}$ 5/2[523]	*E*	*F*
$\pi h_{9/2}$ 1/2[541]	*g*	*h*	$\nu f_{7/2}$ 3/2[521]	*G*	*H*

rations involving the $\frac{7}{2}$[404] or $\frac{7}{2}$[523] proton orbits have significant $\theta_{\rm eq}$ values, at least at the low rotational frequencies, the largest tilt angles being 35° for band $7(\frac{7}{2}[404]_{\pi}\frac{5}{2}[523]_{\nu})$. Of course, these angles move towards 90° as the frequency increases and rotational angular momentum is added along the one axis. This is seen in Fig. 11, which gives the values of $\theta_{\rm eq}$ as a function of rotational frequency. The $K=6$ $\pi h_{11/2}\nu i_{13/2}$ and $\pi g_{7/2}\nu i_{13/2}$ configurations (bands 6 and 1, respectively) have small values of $\theta_{\rm eq}$ initially but show rapidly increasing values as $\hbar\omega$ increases. In contrast the low-*K* couplings of these two configurations (bands 3 and 2, respectively) have $\theta_{\rm eq}$ closer to 90° initially and show more slowly increasing values.

The calculated angular momenta agree well also with the data, as seen in Table VII. The I_3 values are close to the band-head *K* values for the bands of $K=5$ and 6, indicating that the tilted axis of rotation does not affect much the projection on the symmetry axis (*K* is always used here to denote the band-head value). But, there are sizable differences between I_3 and *K* for the low-*K* couplings of these configurations, e.g., bands 2 (2.5$\hbar$ vs 1) and 3 (2.7 and 1). Their trend of I_3 with $\hbar\omega$ is also shown in Fig. 11. Bands 2 and 3 properly have a *K* value close to 1$\hbar$ for very low frequency, but the deviation increases with frequency. Clearly it is more important for these cases to take into account the proper coupling of the angular momenta.

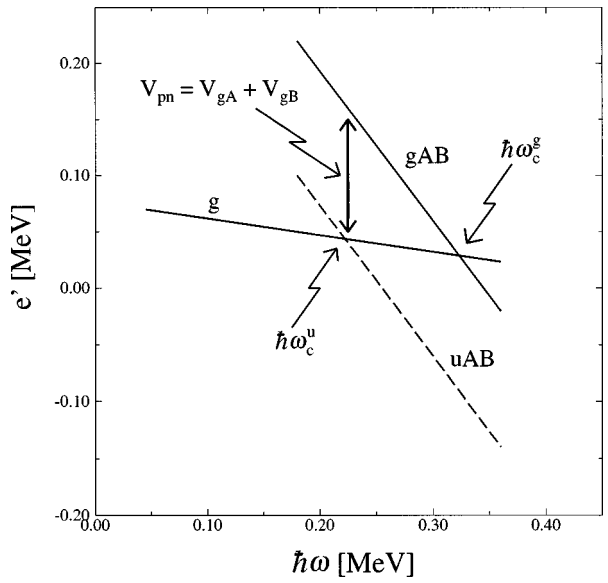

FIG. 9. Schematic Routhian versus rotational frequency for a $\nu i_{13/2}$ (*AB*) crossing in $\pi h_{9/2}$ band (*g*) for an ''unperturbed'' situation (*u* label) and for a realistic situation where the three-quasiparticle band *gAB* is shifted up in energy by the proton-neutron residual interaction V_{pn}. The shift up in energy of the Routhian *gAB* produces a delay in the *AB* crossing frequency, as discussed in the text.

The total angular momentum at $\hbar\omega=0.2$ MeV is calculated as a vectorial sum of the I_1 and I_3 values, listed in column 5 of Table VII, and compared to the experimental values in the last column. Most angular momenta agree well, with the largest deviations being for bands 7 and 9 (1.4 $\hbar$ deviations). While the assignment of band 7 to the $\pi g_{7/2}\nu h_{9/2}$ configuration is clear (as discussed earlier), there is a question about the assignment of band 9.

Also listed in Table VII are the calculated relative energies of the various configurations and the measured energies for the nine observed bands. In the TAC approach, ω is parallel to **I** and is not parallel to $\mathbf{I}_1$ unless $\mathbf{I}_3=0$. For extraction of the Routhian from the data consistent with TAC, the component of the angular momentum perpendicular to ω must be taken to be zero; this is equivalent to setting $K=0$ in the usual PAC formulas. There is good agreement between the order of the predicted and observed configurations. For example, the splitting in energy between the two couplings of $\pi h_{11/2}\nu i_{13/2}$ is calculated to be 256 keV, and the Routhians for bands 6 and 3 differ by 339 keV (see Table V). For the $\pi g_{7/2}\nu i_{13/2}$ configuration the energy difference is predicted to be 285 keV, and measured as 420 keV (bands 1 and 2). In both cases the observed splitting is on the order of 100 keV larger than that calculated by TAC. Of course, the tilted cranking formalism contains no explicit term to take account of the Gallagher-Moszkowski splitting [23] between the parallel (lower) and antiparallel couplings of the intrinsic spins of the two quasiparticle orbits in an odd-odd nucleus. This GM splitting can be on the order of 100 keV, so the differences between experiment and theory in Table VII for these two sets of bands are logical.

Concerning the other bands, the agreement in excitation energy is good, except for bands 4 and 9. The former disagreement is not surprising, since it is well known from studies of odd-*A* nuclei that the $\pi h_{9/2}$ orbit ($\frac{1}{2}$[541]) acts to drive the nucleus to a larger deformation, and this trend is borne out in the band-head deformation calculations of Nazarewicz *et al.* [31]. A uniform deformation of $\epsilon_2=0.247$ was used in the TAC calculations, but the shape calculations indicate that a value at least 9% higher should be used for the $\pi h_{9/2}$ compared to the $\pi h_{11/2}$ orbit for the adjacent odd-*A* Tm nuclei. Using this larger deformation would certainly lower the predicted energy of the $\pi h_{9/2}\nu i_{13/2}$ configurations. As stated above, there is uncertainty in the assignment of the configu-

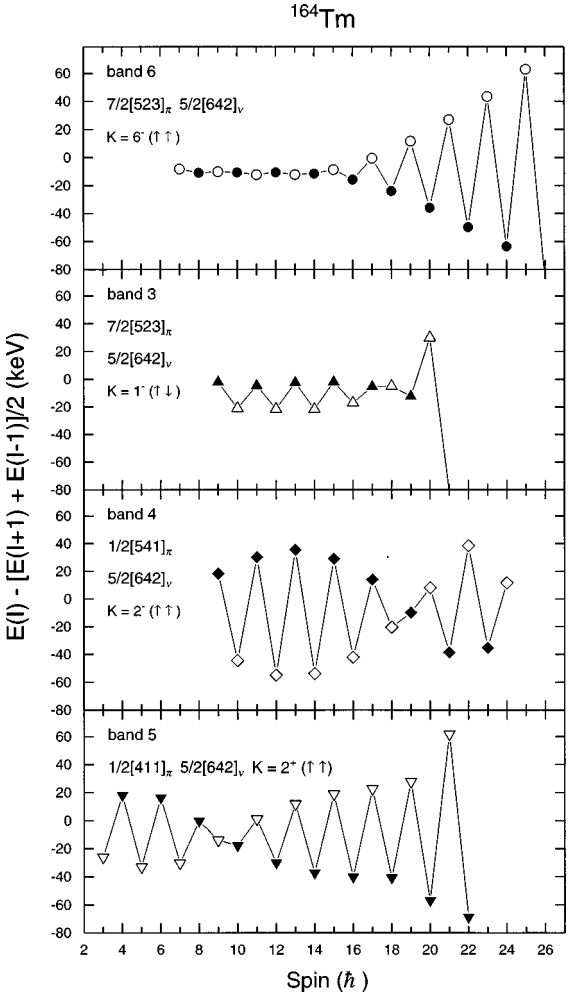

FIG. 10. Energy staggering between the signature partner sequences forming the bands 6, 3, 4, and 5. The favored signature is the one with the lower value of this function. Open symbols being low in staggering indicates a signature inversion over that spin range.

ration for band 9, and even some uncertainty in the experimental placement of the band.

B. Magnetic properties of in-band transitions

The model of tilted axis cranking works well in explaining the energy and angular momentum properties of the seven band structures that exhibit little or no signature splitting in ^{164}Tm, as discussed in the previous section. An analysis of transition probabilities is an even finer test of whether tilted cranking properly accounts for the contributions of the valence proton and neutron spins to the total nuclear spin and its tilt angle to the principal axis.

All nine band structures observed in ^{164}Tm contain $\Delta I=1$ transitions from which the magnetic dipole strength can be extracted, relative to the $E2$ probabilities in each band. The $M1$ transition probabilities are a sensitive measure of the individual g factors of the proton and neutron states in the odd-odd nucleus and of the angular momentum coupling to the total spin I. For example, it is clear which bands involve the $\pi h_{11/2}$ orbital ($\frac{7}{2}[523]$) since it has a g_K value (1.35) that is much larger than that (0.73) for $\pi g_{7/2}$ ($\frac{7}{2}[404]$), resulting in $B(M1)/B(E2)$ values that are bigger. And, it is the coupling of these two orbitals with the $\nu i_{13/2}$ state that leads to axes of rotation substantially tilted relative to the principal axis of the nucleus. The effect of these mechanics on the transition probabilities is clearly important.

The experimental values of $B(M1)/B(E2)$ are extracted from branching ratios under the assumption that the $\Delta I=1$ transitions have pure $M1$ character ($\delta=0$). Since the $E2$ admixtures are always less than 10% (e.g., for bands 3 and 6 only 4%), the uncertainty introduced by this assumption can be neglected compared to the error limits on the branching ratios used. The experimental $B(M1)/B(E2)$ values are shown in Fig. 12 for the bands 6 and 3 ($\pi h_{11/2}\nu i_{13/2}$) and 2 and 1 ($\pi g_{7/2}\nu i_{13/2}$), the former in each set due to the parallel ($\uparrow\uparrow$) coupling of the intrinsic spins and the latter for the anti-parallel ($\uparrow\downarrow$) coupling. Two trends are immediately clear.

Bands 3 and 6, both based on the $\frac{7}{2}[523]_\pi\frac{5}{2}[642]_\nu$ configuration, exhibit larger $M1/E2$ ratios than the set of bands based on the $\frac{7}{2}[404]_\pi\frac{5}{2}[642]_\nu$ configuration. This is expected due to the larger proton g factor for $\pi h_{11/2}$ [$g_K(h_{11/2})>g_K(g_{7/2})$].

More importantly, a comparison between low- and high-K coupling of the proton and neutron spins can be made for the $\pi h_{11/2}\nu i_{13/2}$ configuration. The $B(M1)/B(E2)$ ratios are observed to be smaller for band 6 ($\uparrow\uparrow$) than for band 3 ($\uparrow\downarrow$) since the high-K coupling ($\uparrow\uparrow$) leads to a partial cancellation of the effects on the $M1$ rates from the opposite-sign proton and neutron g factors. Such a $B(M1)/B(E2)$ difference between bands 1 and 2 is not seen, likely because the g factor for the $g_{7/2}$ proton orbital is small, the $M1$ rates are therefore lower, and a measurement of the difference between the parallel and antiparallel couplings is more difficult.

For comparison, TAC calculations of the transition rates have been performed. In this approach, the $M1$ transition strength follows the formula [4]

$$B(M1)=\frac{3}{8\pi}[\sin\theta(I_{3p}+2.91S_{3p}-2.61S_{3n}) -\cos\theta(I_{1p}+2.91S_{1p}-2.61S_{1n})]^2, \quad (5.1)$$

where the components of the angular momenta $I_{p,n}$ on the three- and one-axis and of the corresponding spins $S=\langle s\rangle$ are calculated for the TAC configurations. The free-spin magnetic moments are attenuated by a factor of 0.7. As shown in Fig. 12, the observed trend that the low-K coupling yields larger $B(M1)/B(E2)$ values than the high-K coupling is reproduced by the TAC calculations over the full frequency range. The staggering in the $B(M1)/B(E2)$ values between the signature partners cannot be addressed in TAC without restoring the signature symmetry [32]. This case of ^{164}Tm provides the first test of the transition strengths in the antiparallel coupling and shows that the TAC approach works very well. The slight TAC overprediction of $B(M1)/B(E2)$ ratios for the configurations containing $g_{7/2}$ protons is consistent with somewhat smaller calculated spins compared to data (see Table VII).

C. Magnetic properties of in-band transitions—Comparison to particle-rotor calculations

The success of the tilted cranking model in explaining the $B(M1)/B(E2)$ values in various bands in ^{164}Tm leads to the

TABLE VII. Comparison of tilted-axis cranking calculations with measured features of bands in ^{164}Tm at $\hbar\omega = 0.20$ MeV. The TAC configuration is labeled by the corresponding PAC configuration also calculated at $\hbar\omega = 0.20$ MeV but for $\theta = 90°$. The + and − symbols denote signatures $\alpha = +\frac{1}{2}$ and $-\frac{1}{2}$, respectively.

No.	π Conf.	ν Conf.	I_3 ($\hbar$)	I_1 ($\hbar$)	I ($\hbar$)	θ_{eq} (deg)	E (MeV)	Band	E_{exp} (MeV)	K_{exp} ($\hbar$)	I_{exp} ($\hbar$)
1	$[523]7/2^-$	$[642]5/2^+$	5.4	11.9	13.1	65.8	0.0	6	0	6	13.2
2	$[523]7/2^-$	$[642]5/2^-$	2.7	11.8	12.1	77.3	0.256	3	0.339	1	12.4
3	$[404]7/2^-$	$[642]5/2^+$	5.4	9.4	10.8	60.2	0.300	1	0.127	6	11.9
4	$[411]1/2^-$	$[642]5/2^+$	0.1	11.2	11.2	90	0.308	5	0.235	2	12.1
5	$[523]7/2^-$	$[523]5/2^-$	6.0	8.1	10.1	53.2	0.404	8	0.285	6	10.1
6	$[404]7/2^-$	$[523]5/2^-$	6.0	4.2	7.3	34.8	0.439	7	0.380	6	8.7
7	$[411]1/2^-$	$[642]5/2^-$	0.1	9.8	9.8	90	0.475				
8	$[411]1/2^+$	$[642]5/2^+$	0.2	10.3	10.3	90	0.491				
9	$[404]7/2^-$	$[642]5/2^-$	2.5	9.6	9.9	75.6	0.585	2	0.547	1	11.1
10	$[402]5/2^+$	$[642]5/2^+$	4.1	9.8	10.6	67.1	0.634				
11	$[411]1/2^+$	$[642]5/2^-$	0.0	9.0	9.0	90	0.658				
12	$[523]7/2^-$	$[521]3/2^+$	5.3	8.0	9.6	56.2	0.691	9	0.411	5	11.0
13	$[523]7/2^-$	$[523]5/2^+$	1.4	10.5	10.6	82.6	0.727				
14	$[411]1/2^-$	$[523]5/2^-$	2.5	7.9	8.3	72.2	0.822				
15	$[541]1/2^+$	$[642]5/2^+$	0.1	13.9	13.9	90	0.836	4	0.343	2	12.8
16	$[402]5/2^+$	$[642]5/2^-$	1.6	9.5	9.6	80.2	0.872				
17	$[523]7/2^-$	$[521]3/2^-$	1.7	9.5	9.7	79.8	0.955				
18	$[411]1/2^+$	$[523]5/2^-$	2.2	7.1	7.4	72.8	1.007				
19	$[404]7/2^-$	$[523]5/2^+$	1.3	8.3	8.4	81.3	1.062				

question of whether another model could do as well. Particle-rotor calculations have been performed for ^{164}Tm, mainly with a view towards the energy staggerings and the possible influence of a proton-neutron residual interaction. Full details of the particle-rotor calculations are given below. In the $B(M1)$ calculations, the spin g factor (g_s) for the odd proton and neutron are taken at 70% of their free values (as in the TAC calculations), and the effective g factor for the rotor core (g_R) was taken as 0.35. Figure 13 shows the $B(M1)/B(E2)$ values as a function of spin for the high-K and low-K couplings of the $\pi h_{11/2}\nu i_{13/2}$ configuration, which correspond to observed bands 6 and 3, respectively. Two calculations are shown for each configuration, one including a proton-neutron interaction, and the other without; these are seen to be very similar for both the high-K and low-K configurations. These calculations can be compared to the results of the TAC model which are shown in comparison to the data in Fig. 12 as a function of rotational frequency. The particle-rotor calculations reproduce reasonably well the general tendency of the data for the high-K coupling, and in fact, are rather close to tilted cranking values. Above spin $\sim 18\hbar$ there is a clear staggering in the calculated $B(M1)/B(E2)$ values similar to the staggering seen in the data, and is related to a staggering of the effective alignment of the odd proton when the p-n interaction is included. However, the staggering in the experimental $B(M1)/B(E2)$ values at lower spins is not reproduced, and the reversal of the phase of the staggering is not present in the calculations. For the low-K configuration, the particle-rotor calculations give higher $B(M1)/B(E2)$ values at low spin than for the high-K, as expected, but the calculated $B(M1)/B(E2)$ values decrease too strongly with spin, as compared to both the data and the TAC calculations. This suggests that the low-K band loses its identity too quickly in the particle-rotor model, i.e., that the mixing with other configurations is too strong in this spin range. The particle-rotor calculations provide a reasonable description of the general features of the data, but not in detail.

D. Band crossing in the tilted cranking approach

Tilted-axis cranking affects not only the properties of the band of interest (excitation energy, angular momentum, transition rates) but also possibly the process of rotation alignment of high-j quasiparticles. In ^{164}Tm the observed $\nu i_{13/2}$ alignment process in band 7 provides a good opportunity to test the effect of tilted cranking on a band crossing. The calculated angle of tilt ($\theta_{eq} = 35°$) is larger for this configuration than for any other in ^{164}Tm, and band 7 is the only one with a fully observed $\nu i_{13/2}$ band crossing.

It is worthwhile to investigate the neutron $i_{13/2}$ alignment process in the TAC picture as well and compare it with the result obtained from a principal-axis cranking (PAC) calculation. For this purpose, we have used the same input parameters for deformation and pairing gaps in both types of calculations, identical with the parameter values described previously in Sec. V A. The results are shown in Fig. 14, where the spin versus frequency dependence for band 7 is plotted. The upbend observed around 0.25 MeV is attributed to an alignment of an $\nu i_{13/2}$ pair. The TAC result, indicated by the solid curve, obviously reproduces the experimental crossing frequency, while the PAC result, indicated by the dashed curve, predicts the alignment at a frequency that is about 20 keV lower. This comparison further supports the conclusion that the nucleus in this $\pi g_{7/2}\nu h_{9/2}$ configuration

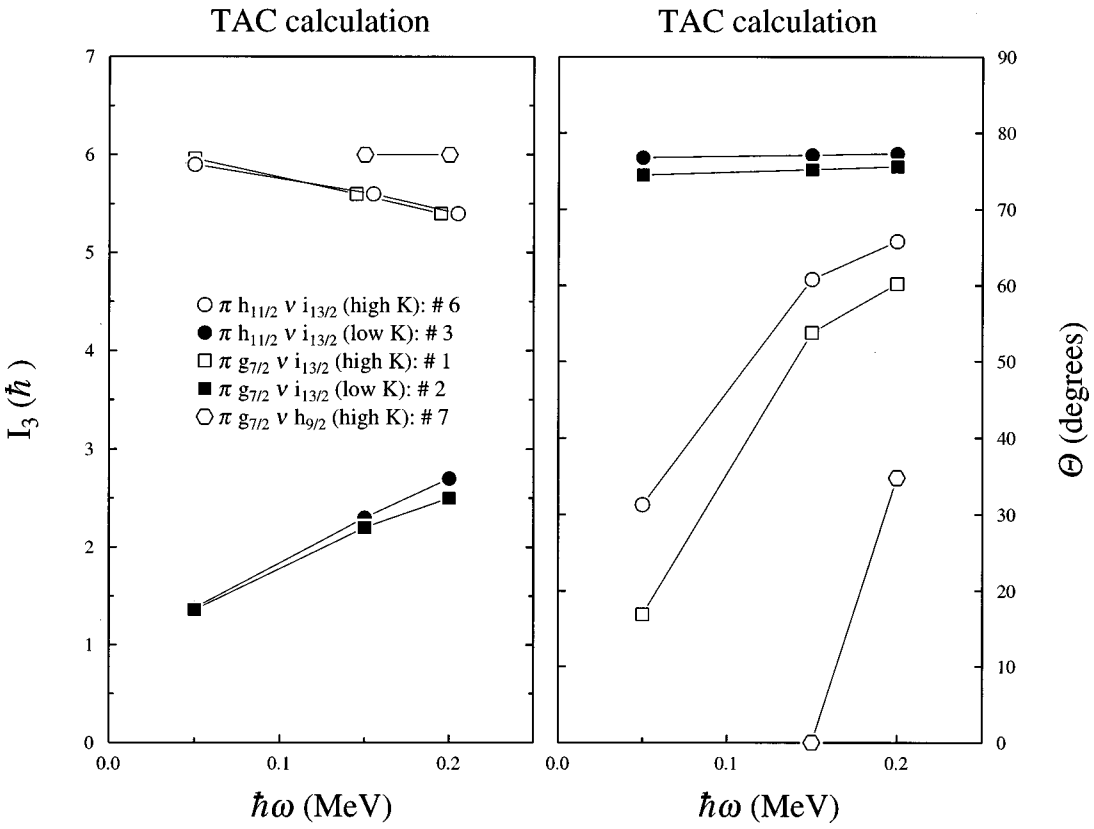

FIG. 11. Calculated spin components I_3 and tilt angles θ for the lowest lying configurations in the tilted cranking scheme. For all configurations, a constant deformation $\epsilon_2 = 0.247$ is assumed. The filled symbols denote the low-K couplings of two configurations, the open symbols high-K bands.

(band 7) rotates around a tilted axis, which results in a delay of the $\nu i_{13/2}$ alignment process.

VI. p-n INTERACTIONS AND THE PARTICLE-ROTOR MODEL

Odd-odd nuclei provide an opportunity to study the effective residual interaction between the unpaired proton and neutron. The selective occurrence of an inversion in the signature for the $\pi h_{9/2} \nu i_{13/2}$ band in ^{164}Tm (see Sec. IV D; also present in ^{162}Tm [8] and ^{174}Ta [10]) has been linked to this p-n residual interaction [10]. In this section we explore signature inversion more deeply in terms of a particle-rotor model, and apply the results to bands not discussed earlier [10].

In the strong coupling limit of the rotational model, the contribution from the p-n interaction to the energy splitting between the rotational bands built on the high-K and low-K couplings of the proton and neutron is denoted the Gallagher-Moszkowski (GM) splitting [23], i.e.,

$$E_{\mathrm{GM}} = \langle K_< | V_{pn} | K_< \rangle - \langle K_> | V_{pn} | K_> \rangle, \qquad (6.1)$$

where $K_> = K_p + K_n$ and $K_< = |K_p - K_n|$. However, a simple analysis of experimental results based on the strong coupling limit is clearly not sufficient when strong configuration mixing is present, e.g., as indicated by large signature splitting or signature inversion. Therefore, calculations have been performed for a number of bands based on the particle-rotor model [33].

In this approach, the model Hamiltonian includes the rotational energy of the core (which can be either axially symmetric or triaxial), the quasiparticle energies of the odd proton and neutron, and a residual p-n interaction. The deformed single particle states were obtained from the modified oscillator potential with the κ,μ parameters from Ref. [34]. The Hamiltonian is diagonalized within the space of low-lying one-quasiproton, one-quasineutron states. Note that the core is assumed to have a fixed shape in this approach, e.g., the γ deformation of the core is required to be the same for signature-partner bands. In the present calculations, a variable moment of inertia (VMI) description of the core energy spectrum was used, with the VMI parameters obtained from an average of the values fitted to the ground bands of the neighboring $Z \pm 1, N \pm 1$ even-even nuclei. The p-n interaction has a standard delta function form

$$V_{pn} = \sqrt{8\pi^3} \left(\frac{\hbar}{m\omega} \right)^{3/2} \delta(\mathbf{r}_p - \mathbf{r}_n)(u_0 + u_1 \sigma_p \cdot \sigma_n), \quad (6.2)$$

with strength parameters $u_0 = -4.95$ MeV and $u_1 = -0.55$ MeV used for all negative-partity calculations with V_{pn} presented here ($\pi h_{9/2} \nu i_{13/2}$ and $\pi h_{11/2} \nu i_{13/2}$ configurations); a stronger interaction ($u_0 = -9.00$ MeV and $u_1 = -1.00$ MeV) is considered for the positive-parity band 5.

First, some details are given for completeness, as well as some justification for the parameters of the p-n interaction. A deformation of $(\varepsilon_2, \varepsilon_4) = (0.27, 0.00)$ was used (triaxiality was shown to be insufficient to explain the inversion), and

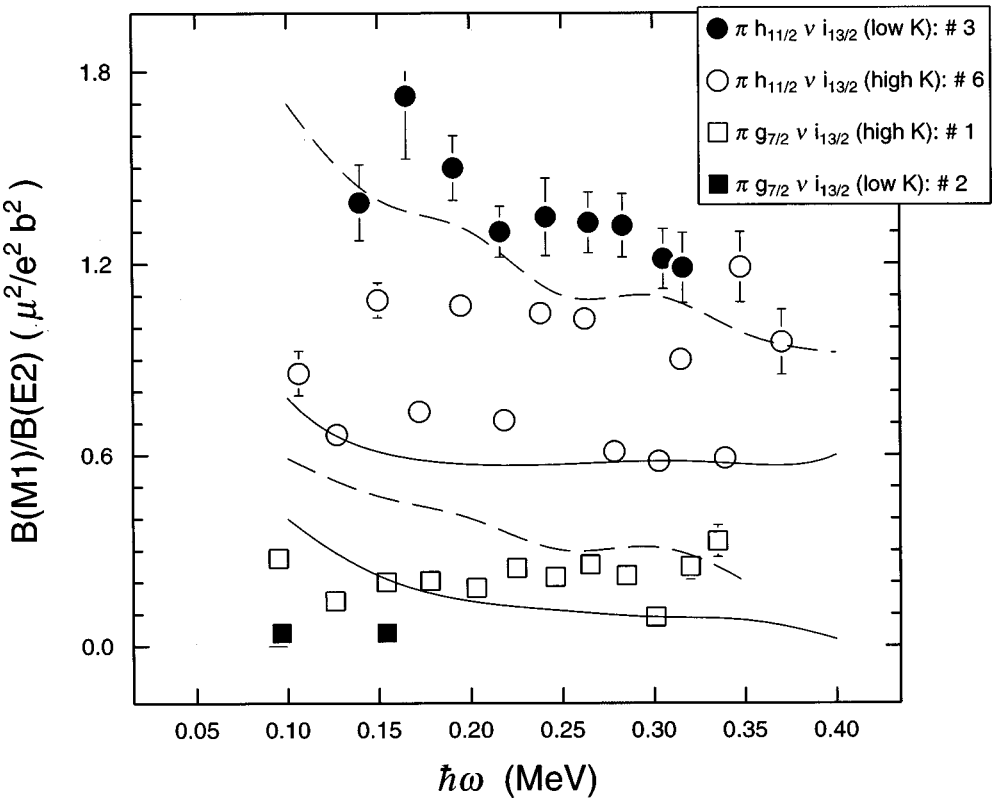

FIG. 12. Experimental $B(M1)/B(E2)$ ratios for the ''doublet'' bands 3 and 6 (circles) and bands 1 and 2 (squares) as a function of rotational frequency and comparison with calculations for two-quasiparticles configurations using the tilted-axis cranking model. For the abscissa values, $\hbar\omega$ is deduced from experiment as described in the text. Theoretical curves: dashed for low-K, full lines for high-K configurations. The upper two curves relate to the $\pi h_{11/2}\nu i_{13/2}$ bands, the lower two to $\pi g_{7/2}\nu i_{13/2}$.

the BCS calculations gave a proton pairing gap $\Delta_p = 0.79$ MeV, and the proton Fermi level about 1.22 MeV below the 1/2[541] Nilsson orbital. The neutron pairing gap was $\Delta_n = 0.74$ MeV, and the Fermi level was about 0.22 MeV above the $\frac{5}{2}$[642] orbital. A Coriolis attenuation factor of 0.80 was used. The parameters used in the p-n interaction are supported by a variety of considerations. The spin-spin strength parameter can be estimated from available GM splittings to be $u_1 = -0.80$ MeV [35,36]; however, the u_0 parameter is not determined from GM splittings since it contributes equally to the energies of the $K_>$ and $K_<$ couplings of a given configuration. A relative strength of the two parameters $u_0 : u_1 = 9:1$ has been suggested from an analysis of $|(j_p \otimes j_n)J\rangle$ multiplets in spherical odd-odd nuclei [37,38], and previous particle-rotor calculations with $u_0 = -7.2$ MeV and $u_1 = -0.80$ MeV gave good results for signature splitting effects in the $\pi h_{11/2}\nu h_{11/2}$ and $\pi h_{11/2}\nu i_{13/2}$ bands in the $A = 130$ and 150 mass regions [7,39,40]. The $\pi h_{9/2}\nu i_{13/2}$ spherical multiplet in ^{210}Bi [41] gives u_0 and u_1 parameters about half as large. Finally, the overall strength of this interaction was adjusted to give approximately the correct inversion spin observed in band 4, while the relative strength $u_0 : u_1 = 9:1$ was kept fixed. Since the final wave functions are not pure $\pi h_{9/2}\nu i_{13/2}$, but about 65%, this V_{pn} is quite reasonable.

For an understanding of how V_{pn} affects the signature splitting, expectation values of the different terms in the Hamiltonian have been computed for the energy eigenvectors. The total energy can be written

$$\langle E_{\rm tot}\rangle = \langle E_{\rm rot}\rangle + \langle E_{qp}\rangle + \langle E_{qn}\rangle + \langle V_{pn}\rangle, \tag{6.3}$$

where $\langle E_{\rm rot}\rangle$ is the energy from the core rotation, $\langle E_{qp}\rangle$ and $\langle E_{qn}\rangle$ are the average quasiparticle energies for the odd proton and neutron, respectively, and $\langle V_{pn}\rangle$ is the average p-n interaction energy. Similarly, the energy staggering can be decomposed as a sum of staggerings of these four quantities. A measure of the alignments of the odd proton and neutron is provided by the expectation values $\langle \mathbf{r}\cdot\mathbf{j}_p\rangle/\sqrt{I(I+1)}$ and $\langle \mathbf{I}\cdot\mathbf{j}_n\rangle/\sqrt{I(I+1)}$, which are also calculated from the particle-rotor eigenfunctions. These quantities are analyzed in detail in different band structures in the following subsections.

A. Band 4: $\pi h_{9/2}\nu i_{13/2}$ configuration

The results of the particle-rotor calculations for this band were briefly summarized in Ref. [10], and additional features of those results are given below. The alignment and energy terms calculated without and with V_{pn} included are shown in Figs. 15 and 16. With no V_{pn} essentially no staggering is seen in the proton alignment, while a clear staggering in the neutron alignment is evident above spin $\sim 7\hbar$ (see Fig. 15). The average quasiparticle energies for the proton and neutron are shown in the middle panel, and a clear staggering in the quasineutron energy has opposite phase to the staggering in

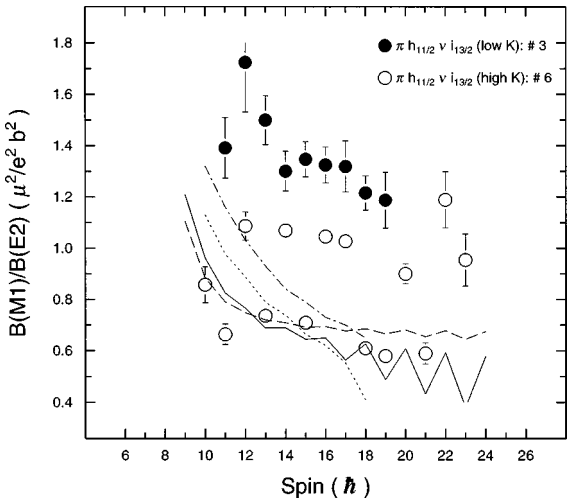

FIG. 13. Experimental $B(M1)/B(E2)$ ratios for the ''doublet'' bands 3 (filled circles) and 6 (open circles) as a function of spin and comparison with calculations for two-quasiparticles configurations using the particle-rotor model. Theoretical curves: full line for the high-K configuration (band 6) with V_{pn} included, dashed with no V_{pn}; dotted line for low-K (band 3) with V_{pn} included, dash-dot with no V_{pn}.

the neutron alignment. This is a natural result, because the more highly aligned neutron occurs for odd spins (the favored signature for an $\pi h_{9/2}\nu i_{13/2}$ configuration) and requires significant low-Ω_n components which are farther from the neutron Fermi surface. However, the cost in higher quasineutron energy is more than offset by the lower rotational energy from the collective core, which is also shown in the middle panel (i.e., less rotation is needed to make the odd spins since the neutron alignment is substantially higher). The staggerings in these energy contributions (defined as $S=E(I)-[E(I+1)+E(I-1)]/2$) are shown in the lowest panel. The staggering in the quasiproton energy is much smaller, indicating that the proton is nearly a spectator, passively occupying the favored signature orbital ($\alpha_p=+1/2$), while the neutron occupies either a favored signature orbital ($\alpha_n=+1/2$, $\alpha_{\rm tot}=1$, odd spin states) or an unfavored signature orbital ($\alpha_n=-1/2$, $\alpha_{\rm tot}=0$, even spin states). Thus, the calculated high-spin behavior is dominated by the staggering in the core rotational energy, with odd spins favored. Qualitatively this agrees with the normal cranking considerations, although the magnitude of the staggering is far too large compared to the data. Note also that at low spins, below $\sim 7\hbar$, the core rotational energy is rather flat, and in fact there is a small inversion in the staggering pattern (even spins favored) calculated for both the core energy and the total energy. Of course, signature inversions have been observed previously in particle-rotor calculations without a p-n interaction and without triaxiality [29,30], but this is clearly insufficient for the present $\pi h_{9/2}\nu i_{13/2}$ band.

Results calculated with the p-n interaction included are shown in Figs. 16 and 17. The effective alignment of the proton, $\langle \mathbf{I}\cdot\mathbf{j}_p\rangle/\sqrt{I(I+1)}$, is very similar to the pattern calculated without any p-n interaction, but the neutron alignment is quite different; the staggering of the neutron alignment at high spins (above $\sim 14\hbar$) is strongly reduced by the inclusion of the p-n interaction, although the odd-spin states still have the greater effective alignment. At lower spins, the phase of the oscillation of the neutron alignment reverses; below $\sim 12\hbar$, the even-spin states have the greater neutron alignment. The average quasiparticle energies, $\langle E_{qp}\rangle$ and $\langle E_{qn}\rangle$, are shown in the next panel, along with the average core rotational energy $\langle E_{\rm rot}\rangle$, and the smoother trend in the neutron alignment pattern is clearly reflected in the smoother quasineutron and rotor energies. Particularly interesting are the $\langle V_{pn}\rangle$ expectation values, which are shown in the middle panel. At the lowest spins, the average p-n interaction is strongly attractive, approximately 350 keV. As the spin increases in the band, there is a gradual loss of this p-n attraction, and a clear staggering in $\langle V_{pn}\rangle$ becomes apparent above spin $\sim 12\hbar$, favoring the even-spin states. The staggerings calculated from these different energy contributions are shown in the bottom panel of Fig. 16, and Fig. 17 shows the total calculated staggering as compared to the experimental data. The general agreement is quite good, although the amplitude of the total staggering is underestimated in the calculations. The qualitative agreement with the data is not sensitive to small changes in the calculations (core moment of inertia, Coriolis attenuation, etc.) but appears for a wide range of reasonable parameter values.

Some interesting aspects of the coupling between the proton, neutron, and core are suggested in the staggerings of the separate energy contributions. At spins above $\sim 14\hbar$, the largest staggerings are due to $\langle E_{\rm rot}\rangle$ and $\langle V_{pn}\rangle$, and these are out of phase (see Fig. 16); $\langle E_{\rm rot}\rangle$ favors the odd spin states, which have the greater neutron alignment, but these are unfavored by $\langle V_{pn}\rangle$. Insight into this staggering of $\langle V_{pn}\rangle$ may be accessible from an expansion of the energy eigenfunctions into the weak coupling basis, i.e., basis states of the form $|(j_p,j_n)J\otimes R;I\rangle$, where a state of total angular momentum I is produced by coupling the proton and neutron angular momenta j_p and j_n to J, which is then coupled to the angular momentum R of the rotor core. By inclusion of the particle and hole amplitudes of the proton and neutron, there are four components associated with this basis state, corresponding to the proton-particle neutron-particle, proton-particle neutron-hole, hole-particle and hole-hole amplitudes. In this basis, the average p-n interaction can be related to the spherical multiplet splittings $\langle (j_p,j_n)J|V_{pn}|(j_p,j_n)J\rangle$. For the $\pi h_{9/2}\nu i_{13/2}$ configuration, empirical matrix elements are available [41]. The proton-particle neutron-particle matrix elements are all negative (attractive), and the related proton-particle neutron-hole matrix elements are all positive (repulsive). The largest matrix elements occur for the low spin $J=2,3$ states and for the stretched state, $J=J_{\rm max}=11$. Thus, the p-n interaction influences not only the size of the vector J but also its *alignment*, through the dependence on the particle and hole character of the participating quasiproton and quasineutron. In the present calculations, the proton Fermi level is about 1.2 MeV below the 1/2[541] Nilsson orbital, and so the quasiproton has nearly pure particle character whether it is deformation aligned (strongly coupled) or rotation aligned. The neutron Fermi level is about 0.2 MeV above the $\frac{5}{2}$[642] Nilsson orbital, and so quasiparticle excitations involving the low-Ω orbitals have large hole character. The low-Ω orbitals are particularly important for building the neutron states with large rotation alignment.

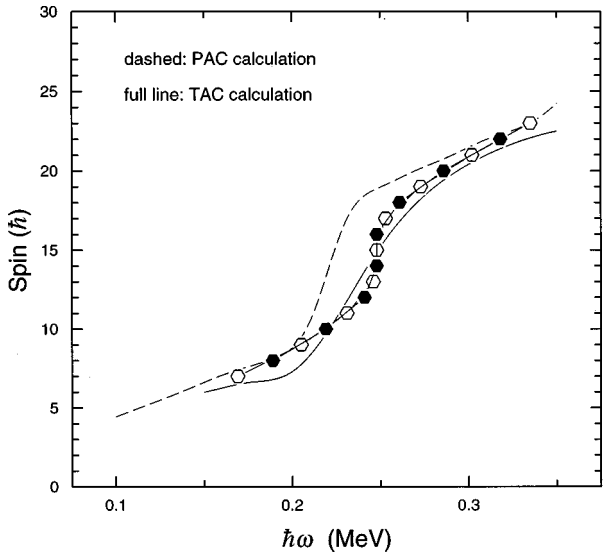

FIG. 14. Spin versus rotational frequency for band 7 (based on $\frac{7}{2}[404]_{\pi}\frac{5}{2}[523]_{\nu}$ configuration). The rotational frequencies for the data have been computed under the assumption of $K=0$. A line connects the experimental points, while the solid calculated line is the result of a tilted-axis calculation and the dashed line is from a principal-axis approach.

Around spin $\sim 24\hbar$ the energy eigenfunctions for the even-spin states have large and nearly equal $J=11$ and $J=10$ components, and both of these components are mainly of particle-particle character. For the odd spin states, the $J=11$ component is nearly twice as large as the $J=10$ component, but has nearly equal particle-particle and particle-hole character. As a result, the $\langle V_{pn}\rangle$ contribution to the total energy is more attractive for the even spin states than for the odd spins, resulting in the strong staggering. Nonetheless, the staggering in $\langle E_{\rm rot}\rangle$ is larger than the staggering in $\langle V_{pn}\rangle$, and the odd spins are favored overall. By comparison, the concentration of the $J=11$ component is much more pronounced in the calculation with no p-n interaction, especially in the odd spin states.

At lower spins, the staggering in $\langle V_{pn}\rangle$ decreases, and becomes less than $\sim\pm 5$ keV below spin $10\hbar$ (and in fact reverses phase, favoring the odd spins). The core rotational energy also reverses phase at low spin, and is the largest contributor to the total energy staggering and thus to the signature inversion. This phase reversal in $\langle E_{\rm rot}\rangle$ is accompanied by reversals in the phase of the staggerings in $\langle E_{qn}\rangle$ and the effective neutron alignment $\langle \mathbf{I}\cdot\mathbf{j}_n\rangle/\sqrt{I(I+1)}$ and thus signals a change in the coupling scheme between the neutron and the core. Below spin $\sim 10\hbar$, both the even and odd spin states still have larger $J=10$ and 11 components than $J=2$ and 3, but the low-J components are clearly more important at the lower total angular momenta. There is also a greater concentration in the low-J components with the p-n interaction included, than without. The wave functions of these semidecoupled states are complicated, especially in the low-spin region where the signature inversion is found, and a simple qualitative description of the coupling scheme and the role of the p-n interaction remains difficult. However, the effect of the p-n interaction is clearly influenced and complicated by the particle and hole character of the participating quasiparticles, and this in turn influences not only the size of the angular momentum J of the proton-neutron pair, but its orientation as well.

B. Bands 3 and 6: $\pi h_{11/2}\nu i_{13/2}$ configurations

1. Band 6: $\pi h_{11/2}\nu i_{13/2}$ high-K

Particle-rotor calculations for the $\pi h_{11/2}\nu i_{13/2}$ configurations were made with the same parameters described for the $\pi h_{9/2}\nu i_{13/2}$ band, except that a slightly smaller deformation ($\varepsilon_2=0.25$) and a stronger Coriolis attenuation (0.60) were used. At this deformation, the BCS calculations gave a proton pairing gap $\Delta_p=0.81$ MeV, and the proton Fermi level about 0.32 MeV above the 7/2[523] Nilsson orbital. The neutron pairing gap was $\Delta_n=0.74$ MeV, and the Fermi level was about 0.33 MeV below the 5/2[642] orbital. The other parameters, including the p-n interaction strengths and VMI core energy spectrum, were the same as described for $\pi h_{9/2}\nu i_{13/2}$ band.

The results for the high-K configuration, with no p-n interaction included, are summarized in Fig. 18. Essentially no staggering is found in any of the displayed quantities below $\sim 12\hbar$, but a small staggering appears above this spin in the proton alignment, quasiproton energy, and rotor energy suggesting that the odd neutron acts as a spectator particle. The larger proton alignment and quasiproton energy occur for even spins, but with a smaller rotor energy.

The calculations for the high-K configuration with the p-n interaction included are shown in Fig. 19 in a manner similar to Fig. 16. The staggering of the proton alignment is much greater with the p-n interaction included than without. In addition, there is a very small staggering in the neutron alignment that was not present without the p-n interaction. At low spins, the average p-n interaction is weakly attractive, $\langle V_{pn}\rangle\sim -60$ keV, but as the spin increases the p-n interaction becomes more strongly attractive, e.g., $\langle V_{pn}\rangle\sim -360$ keV at spin $24\hbar$. The energy staggerings have large oscillations for spins above $\sim 14\hbar$ in the energy contributions from the rotor core, the quasiproton, and the p-n interaction. At high spins, the even-spin states are unfavored by the quasiproton energy, but favored by both the rotor core and the p-n interaction. The opposite tendencies of the quasiproton and rotor energy staggerings are a natural reflection of the larger proton alignment in the even-spin states (the favored signature), but the similar tendencies of the p-n interaction and the rotor energies is opposite to the results calculated for the $\pi h_{9/2}\nu i_{13/2}$ band. The phase of the oscillations in the p-n energy can be qualitatively understood from the weak coupling amplitudes $|(j_p,j_n)J\otimes R;I\rangle$, the particle and hole character of the quasiproton and quasineutron, and the spherical multiplet splittings $\langle(j_p,j_n)J|V_{pn}|(j_p,j_n)J\rangle$. Similar to the $\pi h_{9/2}\nu i_{13/2}$ configuration, all of the proton-particle, neutron-particle $\langle(j_p,j_n)J|V_{pn}|(j_p,j_n)J\rangle$ matrix elements for the $\pi h_{11/2}\nu i_{13/2}$ configuration are calculated to be attractive, with the largest matrix elements (in magnitude) for the low spin $J=1,2$ states and for the stretched state, $J=J_{\rm max}=12$. Around spin $20\hbar$, the largest weak coupling amplitudes occur for $J=11$ and $J=12$. For the even-spin states, the $J=12$ amplitudes are the largest, and are mainly of proton-hole, neutron-hole character, which results in a strongly at-

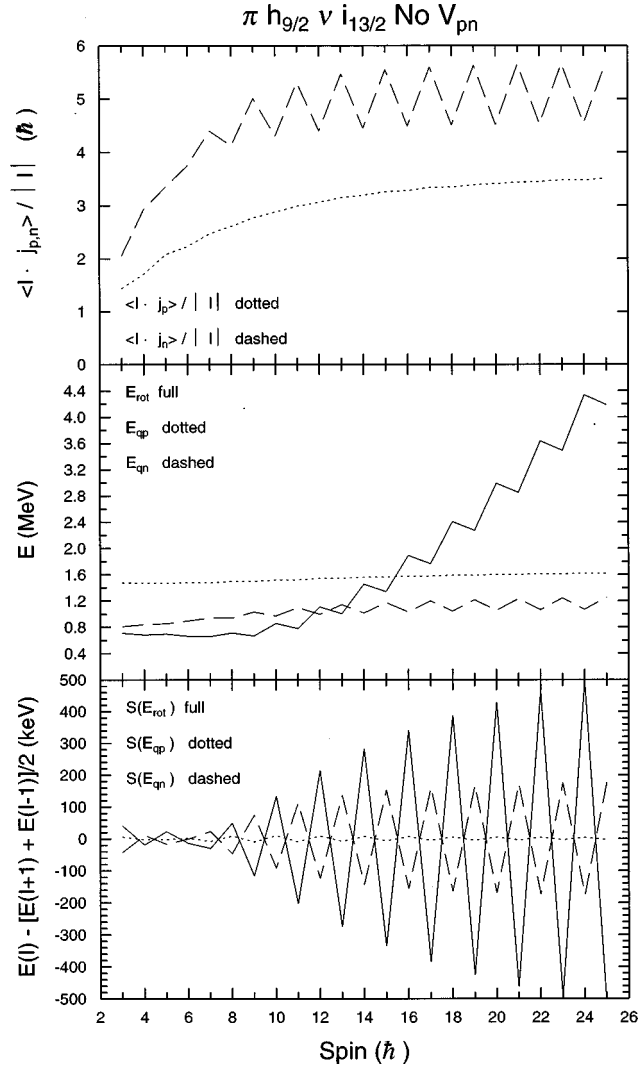

FIG. 15. Particle-rotor calculations (with no p-n interaction included) for the $\pi h_{9/2}\nu i_{13/2}$ band of (top panel) proton and neutron ''alignments'' as a function of spin; (middle panel) contributions to the calculated energy from rotation and from the proton and neutron [see Eq. (6.3)]; and energy staggerings for each of these three components.

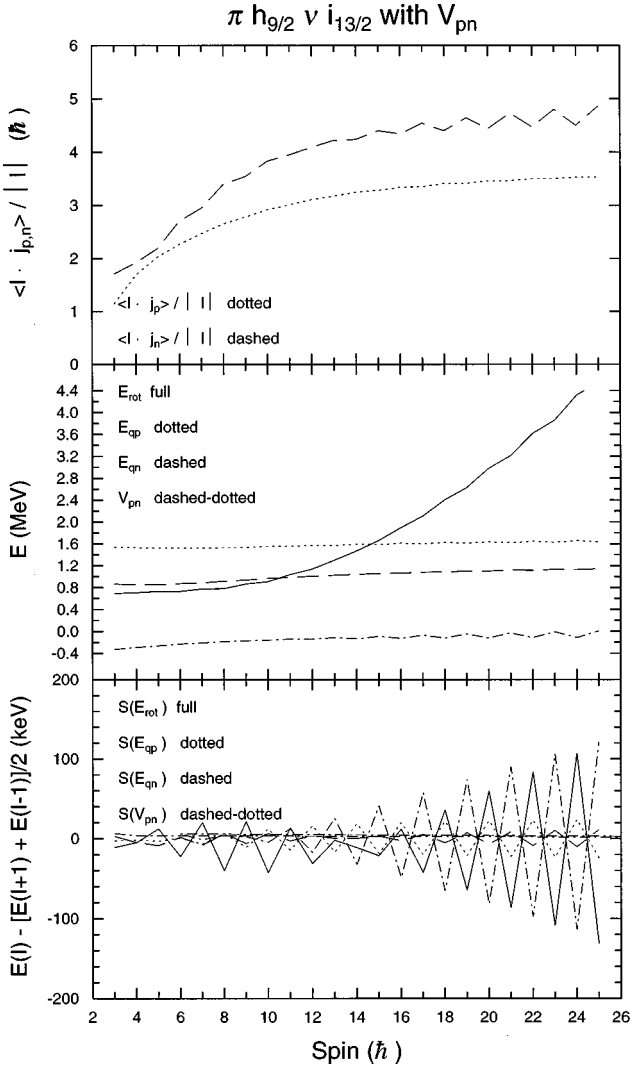

FIG. 16. Particle-rotor calculations, with the p-n interaction included, of the same quantities as in Fig. 15, for the $\pi h_{9/2}\nu i_{13/2}$ band.

tractive $\langle V_{pn}\rangle$ contribution. For the odd-spin states, the $J=12$ components are smaller, and are slightly less than the $J=11$ components. Consequently, the $\langle V_{pn}\rangle$ contribution is much less attractive for the odd-spin states than for the even spins. Comparing the calculations with and without the p-n interaction at spin $\sim 20\hbar$, those including $\langle V_{pn}\rangle$ have a slightly greater concentration of the $J=11$ and $J=12$ components in the wave function (compared to the lower J components), but a noticeably greater concentration of the $J=12$ component compared to the $J=11$ for the even-spin states. Thus, for the yrast $\pi h_{11/2}\nu i_{13/2}$ band, the p-n interaction increases the staggering of the alignment of the odd proton, but the expected larger splitting in the total energy is somewhat offset by the staggering in the $\langle V_{pn}\rangle$. For the lower spin states, the $J=11$ and $J=12$ weak coupling components are smaller than for higher spins, but are still the largest, even around $\sim 8\hbar$. At these low spins, the wave functions calculated with and without the p-n interaction are very similar.

The experimental and calculated energy staggerings for this band are displayed in Fig. 17 (top). The staggering is slightly overestimated in the calculations including the p-n interaction, and strongly underestimated without it. However, the overall effect of the p-n interaction on the energy staggering is rather small, and with the same p-n interaction that was adjusted to the signature inversion in the $\pi h_{9/2}\nu i_{13/2}$ band, the overall agreement with the data is very good.

2. Band 3: $\pi h_{11/2}\nu i_{13/2}$ low-K

The particle-rotor calculations for the low-K coupling of the $\pi h_{11/2}\nu i_{13/2}$ configuration indicate cancellations between quasiproton and core-rotation energies similar to the mechanisms previously described for the high-K coupling. Thus, only the staggerings of the total energy are shown in the present case (Fig. 17). The calculations without the p-n interaction suggest that the odd neutron is effectively a spectator particle in the unfavored signature orbital, and the two signature branches of this band are mainly formed by the $\alpha_p=\pm\frac{1}{2}$ orbitals of the odd proton coupled to the $\alpha_n=-\frac{1}{2}$ neutron orbital. In this simplified picture, the favored signature should correspond to the favored signature of the proton

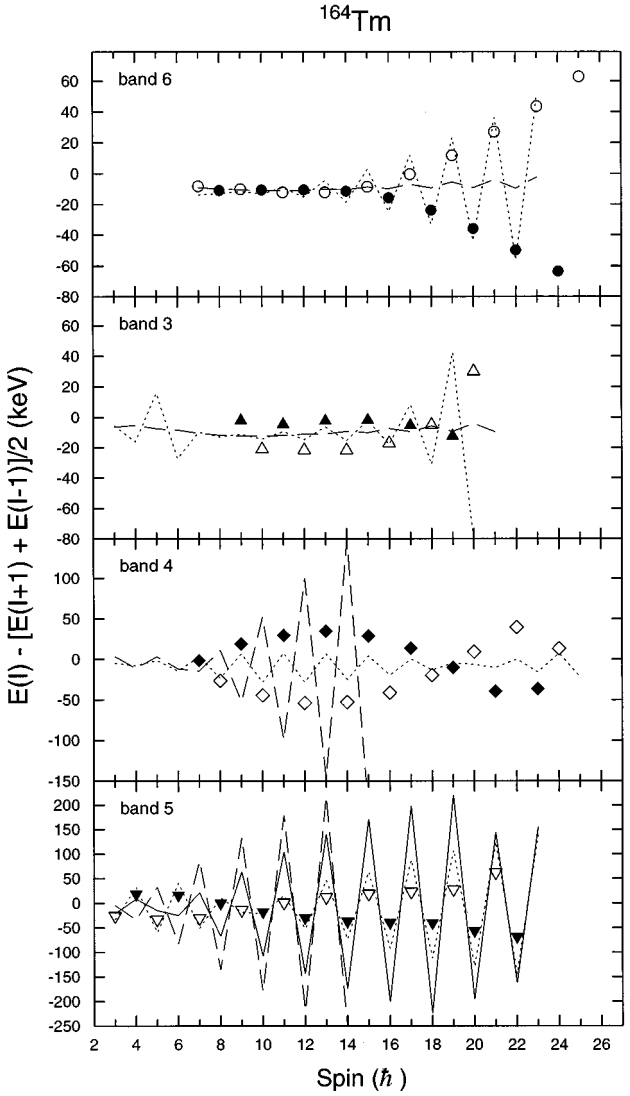

FIG. 17. Comparison of the observed energy staggering of the total energy with the results of the particle-rotor calculations with the p-n interaction included (dotted line) and not included (dashed line), for the $\pi h_{11/2}\nu i_{13/2}$ $K=6$ band (top panel: band 6), the $\pi h_{11/2}\nu i_{13/2}$ $K=1$ band (second panel: band 3), for the $\pi h_{9/2}\nu i_{13/2}$ band (third panel: band 4), and for the $\pi d_{3/2}\nu i_{13/2}$ band (bottom panel: band 5). For band 5, the solid line corresponds to a calculation with the same V_{pn} as used in the other calculations, while the dotted line represents a calculation with a stronger V_{pn}—see text.

($\alpha_p=-\frac{1}{2}$ for $h_{11/2}$) coupled to the $\alpha_n=-\frac{1}{2}$ spectator neutron, which would result in the odd spin sequence as the favored branch. However, the rotor and quasiproton staggerings are overall small and nearly cancel completely below spin $\sim 16\hbar$, i.e., over almost the whole spin range observed experimentally.

When the p-n interaction is included, the staggering pattern of the effective proton alignment is reversed, with the even spins having the slightly larger proton alignment. This is also evident in the staggering of the different energies, where, similar to the high-K case, the higher quasiproton energy but lower $\langle V_{pn}\rangle$ and core rotational energies occur for the even spins. The experimental and calculated total energy staggerings for this band are displayed in the second panel of Fig. 17. Between spins 9 and 17$\hbar$, the calculations without a p-n interaction indicate a weak staggering with the odd spins favored, while both the data and the calculation with the p-n interaction show the even spins favored. At spin 18$\hbar$, the oscillation changes phase in the experiment, but not in the calculations. The disagreement with the calculations including the p-n interaction for spins above 18 is due to a crossing with another band with a much larger alignment. This feature depends sensitively on the details of the calculation, e.g., a somewhat weaker V_{pn} does not produce this clear disagreement, but the general staggering in the energy and the favoring of the even spins does remain for a wide range of parameter values. Recalling that the V_{pn} parameters were adjusted for the $\pi h_{9/2}\nu i_{13/2}$ band, the general level of agreement for these $\pi h_{11/2}\nu i_{13/2}$ bands is quite remarkable.

C. Band 5: $\pi d_{3/2}\nu i_{13/2}$ configuration

The energy staggering for band 5 is shown in the bottom panel of Fig. 10, and the corresponding particle-rotor calculations are shown in Fig. 17. For the calculations with no p-n interaction, the odd proton is effectively confined to the $\frac{1}{2}[411]$ Nilsson orbital (with $<1\%$ admixture of other components up to $I=14\hbar$), while the aligning odd neutron spreads over the available $i_{13/2}$ orbitals. The resulting energy staggering has the correct phase at high spins (with even spins favored), although the amplitude of the staggering is too large. The inversion at low spins is not present in these calculations.

When the p-n interaction is included, the staggering at high spins is reduced and a signature inversion is obtained, as shown in the bottom panel of Fig. 17. However, only a modest improvement is found with the same p-n interaction as used previously for the $\pi h_{9/2}\nu i_{13/2}$ and the $\pi h_{11/2}\nu i_{13/2}$ configurations ($u_0=-4.95$ MeV and $u_1=-0.55$ MeV); the calculated inversion spin is too low and the staggering at high spins is still too large. Both of these features are improved by increasing the strength of the interaction, and excellent agreement with the data is obtained with $u_0=-9.00$ MeV and $u_1=-1.00$ MeV (dotted line). In this case, the calculated proton wave functions are still dominated by the $\frac{1}{2}[411]$ components, but the odd-spin states now have significant $\frac{3}{2}[411]$ admixtures as well ($\sim 8\%$ for $I=7\hbar$). The $|(j_p,j_n)J\otimes R;I\rangle$ decomposition may be useful here even though there is greater mixing between the proton j shells. For the calculations without the p-n interaction, the $\pi d_{3/2}\nu i_{13/2}$ components account for $\sim 45\%$ of the wave functions for both even and odd spins (I), but with the p-n interaction included the $\pi d_{3/2}\nu i_{13/2}$ components are somewhat smaller for the odd-I states ($\sim 40\%$ for $I=7\hbar$), reflecting the mixing with the 3/2[411] orbital. Also, above $I=5\hbar$ the largest $\pi d_{3/2}\nu i_{13/2}$ components for the even-I and odd-I states are the stretched $J=J_{\max}=8$ and the antialigned $J=J_{\min}=5$ components, respectively, with or without the p-n interaction. However, there is a clear difference for the $I=3,4,5$ states: with no p-n interaction, the $J_{\max}=8$ components are largest, but with the p-n interaction, the $J_{\min}=5$ components are largest.

This analysis suggests that a stronger p-n interaction is appropriate for this positive-parity band, and a comparison of the GM splittings of the $\pi\frac{1}{2}[411]\nu 7/2[633]$ $K=3,4$ doublet and the $\pi\frac{7}{2}[523]\nu 7/2[633]K=0,7$ doublet supports this.

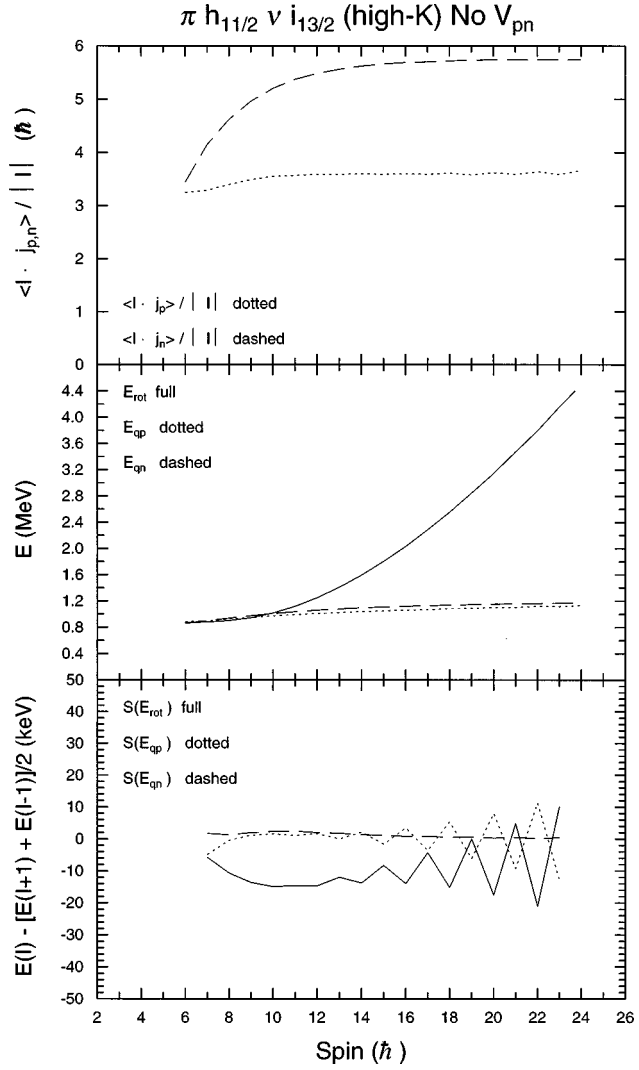

FIG. 18. Particle-rotor calculations (with no p-n interaction included) of the same quantities as in Fig. 15 for the $\pi h_{11/2}\nu i_{13/2}$ $K=6$ band.

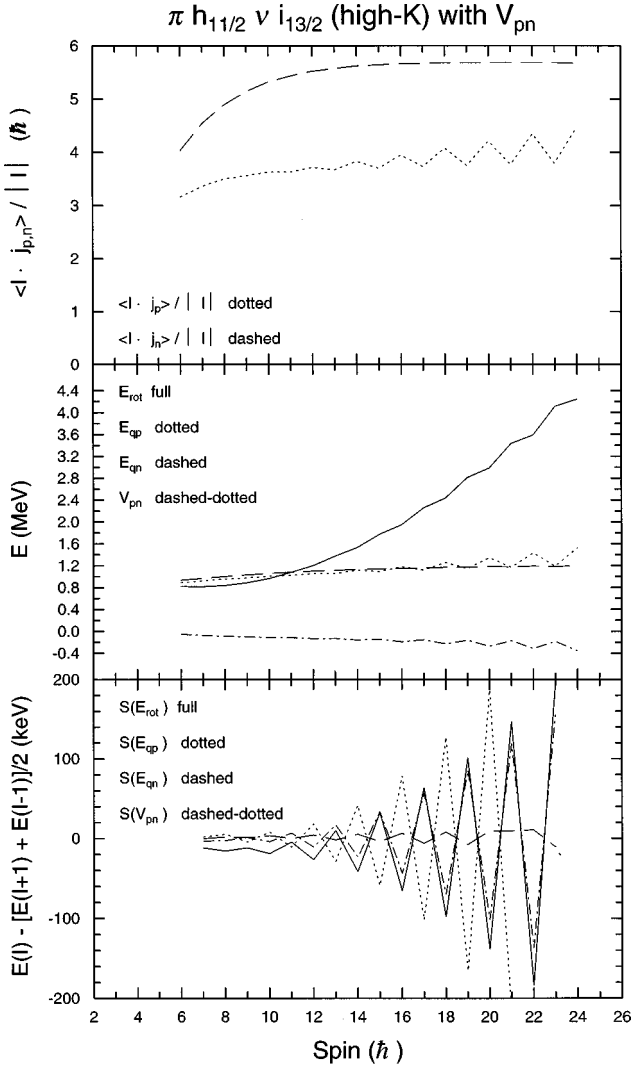

FIG. 19. Particle-rotor calculations, with the p-n interaction included, of the same quantities as in Fig. 18, for the $\pi h_{11/2}\nu i_{13/2}$ $K=6$ band.

Empirical values are tabulated in Ref. [36], and these particular observables are better described with the two different p-n interactions used here that were adjusted to the staggering patterns of the $\pi h_{9/2}\nu i_{13/2}$ and $\pi d_{3/2}\nu i_{13/2}$ bands. Thus, the stronger p-n interaction which provides an excellent description of the energy staggering for band 5 seems reasonable.

VII. CONCLUSIONS

Nine rotational bands have been assigned in odd-odd ^{164}Tm, building upon and greatly extending the earlier work of Drissi *et al.* [2]. For the first time, bands built on the parallel and antiparallel couplings of the intrinsic proton and neutron spins have been seen, for both the $\pi h_{11/2}\nu i_{13/2}$ and the $\pi g_{7/2}\nu i_{13/2}$ configurations. These two sets of $K=1$ and 6 bands provide a rich opportunity to test the predictions of particle-rotor and tilted-cranking calculations. We find that the $B(M1)/B(E2)$ values in the higher-lying $K=1$ $(\uparrow\downarrow)$ coupling for $\pi h_{11/2}\nu i_{13/2}$ are 50% higher than those in the parallel coupling.

This large enhancement in the $M1$ rates is a natural result because the spin magnetic dipoles of the proton and neutron add constructively for the antiparallel coupling of their intrinsic spins, and is nicely reproduced by the tilted-axis cranking calculations (see Fig. 12). The overall success in explaining the branching ratios in the tilted cranking calculation is a clear demonstration of the importance of non-principal-axis cranking at even the two-quasiparticle level in this region of strong deformation.

A remaining puzzle in the measured branching ratios for ^{164}Tm is a substantial staggering in the $B(M1)/B(E2)$ values for the $K=6$ $\pi h_{11/2}\nu i_{13/2}$ band (the most strongly populated structure), in the spin range of 10 to 23$\hbar$ (see Fig. 13). This staggering is surprising, since there is essentially no energy splitting between the signatures of band 6 (see Fig. 8). Neither the particle-rotor nor the tilted cranking calculations could produce $B(M1)/B(E2)$ oscillations at these spins.

Another significant observation is the large signature inversion in the $\pi h_{9/2}\nu i_{13/2}$ band in ^{164}Tm. Regular inversions have been seen in the $\pi h_{11/2}\nu i_{13/2}$ bands in lighter Tm and other nuclei, but the amplitude of this inversion has de-

creased to zero in ^{164}Tm ($N=95$). The large inversion in the $\pi h_{9/2}\nu i_{13/2}$ band (up to $I=18\hbar$) is therefore surprising. Furthermore, the small but clear signature inversion in the $K=1$ coupling of $\pi h_{11/2}\nu i_{13/2}$ had not been seen before.

The selective appearance of signature inversions in ^{164}Tm is well described by our particle-rotor calculations including a simple proton-neutron interaction (a two-parameter delta interaction). The underlying mechanism is complicated because a number of factors influence the coupling scheme $|(j_p,j_n)J\otimes R;I\rangle$ in which the proton, neutron, and rotor core are coupled to a total angular momentum I. Among the factors that influence the coupling are the rotor energies, the Coriolis coupling between the particles and the core, the proton and neutron quasiparticle energies, and the p-n interaction. The effect of the p-n interaction is strongly modified by the particle and the hole character of the proton and neutron quasiparticle excitations, because the V_{pn} matrix elements are attractive for a proton-particle neutron-particle pair, but are repulsive for a proton-particle neutron-hole pair. One of the largest magnitude V_{pn} matrix elements occurs for the stretched configuration ($J=J_{\max}=j_p+j_n$), which is particularly important for high-spin states. In the $\pi h_{9/2}\nu i_{13/2}$ band, the $h_{9/2}$ proton is essentially a particle state, while an aligned $i_{13/2}$ neutron requires large hole amplitudes. Consequently an aligned $J=J_{\max}=11\hbar$ configuration is unfavored by the p-n interaction, and a sizeable signature inversion occurs in the calculations, in good agreement with the data. Similar inversions are found in experiments on ^{162}Tm [8] and ^{174}Ta [10]. For the $\pi h_{11/2}\nu i_{13/2}$ bands, both particle and hole amplitudes can be important for the proton excitations as well as for the neutron. The overall effect of the p-n interaction is less obvious than in the $\pi h_{9/2}\nu i_{13/2}$ band, but the agreement with the data is quite good. Thus, the effect of the p-n interaction is modified by the particle and hole character of the quasiparticle excitations, which in turn influences the magnitude and the orientation of the angular momentum J of the proton-neutron pair.

The particle-rotor calculations presented here clearly demonstrate that the proton-neutron interaction can be a major factor in the signature-splitting–signature-inversion of a two-quasiparticle band, but it is not necessarily the most important factor (as illustrated by the strong effect in the $\pi h_{9/2}\nu i_{13/2}$ band, but the much smaller effect in the $\pi h_{11/2}\nu i_{13/2}$ bands). In some cases, effects not included here may be very important, e.g., triaxiality and, in spite of the very good quality of the energy calculations in the particle-rotor model, the more modest agreement with the experimental $B(M1)/B(E2)$ values suggests that improvements are still possible. For the high-K $\pi h_{11/2}\nu i_{13/2}$ band, the general magnitude and trend of the $B(M1)/B(E2)$ values are rather well described but not the staggering, even though the energy staggerings are well described. Also, the magnitude of the $B(M1)/B(E2)$ values was underestimated for the low-K $\pi h_{11/2}\nu i_{13/2}$ band. These discrepancies suggest that the $M1$ rates are sensitive to fine details in the wave function that are not yet sufficiently well determined in the particle-rotor calculations (e.g., the evolution and oscillation of the proton and neutron alignments as the band progresses to higher spin). In contrast, the tilted-axis cranking calculations are able to describe the general trends of the $B(M1)/B(E2)$ data for both the high-K and the low-K $\pi h_{11/2}\nu i_{13/2}$ bands, although the TAC approach cannot address the signature staggerings in either the energies or the $B(M1)/B(E2)$ values unless the $D2$ symmetry, responsible for the signature quantum number in the common principal-axis cranking (PAC), is restored. Work in this direction is now underway [32], and it will be very interesting to find whether the signature-restored tilted-axis cranking model can provide a good description and understanding of these signature effects. Odd-odd nuclei, though difficult from both the experimental and theoretical viewpoints, provide the simplest multiquasiparticle states available for study and thus are rich prospects for testing nuclear models, as shown in this paper.

ACKNOWLEDGMENTS

The authors wish to acknowledge valuable discussions with F. Dönau and S. Frauendorf, and the help of H. Q. Jin with the discussion of results and analysis of trends. The hospitality and support of the staff of the Niels Bohr Institute Tandem Accelerator Laboratory was crucial for performing the experiments described in this paper. This work was supported by the U.S. Department of Energy under Contracts No. DE-FG02-96ER40983 (University of Tennessee) and DE-FG05-92ER40694 (Tennessee Technological University), the Danish Natural Science Foundation, and the Nordball Collaboration.

[1] R. Bengtsson and S. Frauendorf, Nucl. Phys. **A314**, 27 (1979); **A327**, 139 (1979).

[2] S. Drissi, J.-Cl. Dousse, V. Ionescu, J. Kern, J.-A. Pinston, and D. Barnéoud, Nucl. Phys. **A466**, 385 (1987), and references therein.

[3] A. Brockstedt, J. Lyttkens-Linden, M. Bergström, L. P. Ekström, H. Ryde, J. C. Bacelar, J. D. Garrett, G. B. Hagemann, B. Herskind, F. R. May, P. O. Tjøm, and S. Frauendorf, Nucl. Phys. **A571**, 337 (1994).

[4] S. Frauendorf, Nucl. Phys. **A577**, 295c (1993), and references therein.

[5] R. Bengtsson, H. Frisk, F. R. May, and J.-A. Pinston, Nucl. Phys. **A415**, 189 (1984).

[6] S. Drissi, A. Bruder, J.-Cl. Dousse, V. Ionescu, J. Kern, J.-A. Pinston, S. André, D. Barnéoud, J. Genevey, and H. Frisk, Nucl. Phys. **A451**, 313 (1986).

[7] P. B. Semmes and I. Ragnarsson, *Proceedings of the International Conference on High-Spin Physics and Gamma-Soft Nuclei*, Pittsburgh, 1990, edited by J. X. Saladin, R. A. Sorenson, and C. M. Vincent (World Scientific, Singapore, 1991), p. 500.

[8] J. M. Espino, G. B. Hagemann, I. G. Bearden, R. A. Bark, M. Bergström, A. Bracco, B. Herskind, H. J. Jensen, S. Leoni, C. Martinez-Torre, B. Million, and P. O. Tjøm, Nucl. Phys. **A640**, 163 (1998).

[9] R. A. Bark, H. Carlsson, S. J. Freeman, G. B. Hagemann, F. Ingbretsen, H. J. Jensen, T. Lönnroth, M. J. Piiparinen, I. Rag-

narsson, H. Ryde, H. Schnack-Petersen, P. B. Semmes, and P. O. Tjøm, Nucl. Phys. **A630**, 603 (1998).
[10] R. A. Bark, J. M. Espino, W. Reviol, P. B. Semmes, H. Carlsson, I. G. Bearden, G. B. Hagemann, H. J. Jensen, I. Ragnarsson, L. L. Riedinger, H. Ryde, and P. O. Tjøm, Phys. Lett. B **406**, 193 (1997); **416**, 453(E) (1998).
[11] P. Juneja, S. L. Gupta, S. C. Pancholi, A. Kumar, D. Mehta, L. Chaturvedi, S. K. Katoch, S. Malik, G. Shanker, R. K. Bhowmik, S. Muralithar, G. Rodrigues, and R. P. Singh, Phys. Rev. C **53**, 1221 (1996).
[12] K. Hara and Y. Sun, Nucl. Phys. **A531**, 221 (1991).
[13] W. Reviol, L. L. Riedinger, X. Z. Wang, J.-Y. Zhang, H. J. Jensen, G. B. Hagemann, R. A. Bark, P. O. Tjøm, S. Leoni, T. Lönnroth, H. Schnack-Petersen, T. Shizuma, and J. Wrzesinski, Proceedings of the Conference on Nuclear Structure at the Limits, Argonne, 1996, Report No. ANL/PHY-97/1, p. 165.
[14] L. L. Riedinger, H. Q. Jin, W. Reviol, J.-Y. Zhang, R. A. Bark, G. B. Hagemann, and P. B. Semmes, Prog. Part. Nucl. Phys. **38**, 251 (1997).
[15] S. André, D. Barnéoud, C. Foin, J. Genevey, J.-A. Pinston, B. Haas, J. P. Vivien, and A. J. Kreiner, Z. Phys. A **333**, 247 (1989).
[16] S. Drissi, A. Bruder, M. Carlen, J.-Cl. Dousse, M. Gasser, J. Kern, S. J. Mannanal, B. Perny, Ch. Rheme, J. L. Salicio, J. P. Vorlet, and I. Hamamoto, Nucl. Phys. **A543**, 495 (1992).
[17] S. J. Mannanal, B. Boschung, M. Carlen, J.-Cl. Dousse, S. Drissi, P. E. Garrett, J. Kern, B. Perny, Ch. Rheme, J. P. Vorlet, C. Gunther, J. Manns, and U. Muller, Nucl. Phys. **A582**, 141 (1995).
[18] S. Drissi, S. André, D. Barnéoud, C. Foin, J. Genevey, and J. Kern, Nucl. Phys. **A601**, 234 (1996).
[19] G. Sletten, J. Gascon, and J. Nyberg, Proceedings of the International Conference on Spectroscopy of Heavy Nuclei, Crete, Greece, 1989, Int. Phys. Ser. No. 105 (unpublished).
[20] C. M. Lederer and V. S. Shirley, *Table of Isotopes*, 7th ed. (Wiley, New York, 1978).
[21] D. C. Radford, Nucl. Instrum. Methods Phys. Res. A **361**, 297 (1995).
[22] H. J. Jensen, G. B. Hagemann, P. O. Tjøm, S. Frauendorf, A. Atac, M. Bergström, A. Bracco, A. Brockstedt, H. Carlsson, P. Ekström, J. M. Espino, B. Herskind, F. Ingebretsen, J. Jongman, S. Leoni, R. M. Lieder, T. Lönnroth, A. Maj, B. Million, A. Nordlund, J. Nyberg, M. Piiparinen, H. Ryde, M. Sugawara, and A. Virtanen, Z. Phys. A **340**, 351 (1991).
[23] C. J. Gallagher and S. A. Moszkowski, Phys. Rev. **111**, 1282 (1958).
[24] J. D. Garrett, O. Andersen, J. J. Gaardhøje, G. B. Hagemann, B. Herskind, J. Kownacki, J. C. Lisle, L. L. Riedinger, W. Walus, N. Roy, S. Jonsson, H. Ryde, M. Guttormsen, and P. O. Tjøm, Phys. Rev. Lett. **47**, 75 (1981).
[25] H. J. Jensen, R. A. Bark, R. Bengtsson, G. B. Hagemann, P. O. Tjøm, S. Y. Araddad, C. W. Beausang, R. Chapman, J. Copnell, A. Fitzpatrick, S. J. Freeman, S. Leoni, J. C. Lisle, J. Simpson, A. G. Smith, D. M. Thompson, S. J. Warburton, and J. Wrzesinski, Z. Phys. A **359**, 127 (1997).
[26] S. Frauendorf, L. L. Riedinger, J. D. Garrett, J. J. Gaardhøje, G. B. Hagemann, and B. Herskind, Nucl. Phys. **A431**, 511 (1984).
[27] H. J. Jensen and R. A. Bark, Acta Phys. Pol. B **26**, 271 (1995).
[28] Y. Liu, Y. Ma, H. Yang, and S. Zhou, Phys. Rev. C **52**, 2514 (1995).
[29] A. J. Kreiner and M. A. J. Mariscotti, J. Phys. G **6**, L6 (1980).
[30] I. Hamamoto, Phys. Lett. B **193**, 399 (1987).
[31] W. Nazarewicz, M. A. Riley, and J. D. Garrett, Nucl. Phys. **A512**, 61 (1990).
[32] F. Dönau, J.-Y. Zhang, and L. L. Riedinger, Phys. Lett. B (to be published).
[33] I. Ragnarsson and P. B. Semmes, Hyperfine Interact. **43**, 425 (1988).
[34] T. Bengtsson and I. Ragnarsson, Nucl. Phys. **A436**, 14 (1985).
[35] J. P. Boisson, R. Piepenbring, and W. Ogle, Phys. Rep., Phys. Lett. **26C**, 99 (1976).
[36] D. Nosek, J. Kvasil, R. K. Sheline, P. C. Sood, and J. Noskova, Int. J. Mod. Phys. E **3**, 967 (1994).
[37] M. Moinester, J. P. Schiffer, and W. P. Alford, Phys. Rev. **179**, 984 (1969).
[38] J. P. Schiffer, Ann. Phys. (N.Y.) **66**, 798 (1971).
[39] B. Cederwall, F. Liden, A. Johnson, L. Hildingsson, R. Wyss, B. Fant, S. Juutinen, P. Ahonen, S. Mitarai, J. Mukai, J. Nyberg, I. Ragnarsson, and P. B. Semmes, Nucl. Phys. **A542**, 454 (1992).
[40] N. Tajima, Nucl. Phys. **A572**, 365 (1994).
[41] J. P. Schiffer and W. W. True, Rev. Mod. Phys. **48**, 191 (1976).
[42] A. Bohr and B. Mottelson, *Nuclear Structure* (Benjamin, New York, 1975), Vol. 2.
[43] M. I. Baznat, N. I. Pyatov, and M. I. Chernei, Sov. J. Nucl. Phys. **19**, 135 (1974).